ASTRONOMY & ASTROPHYSICS
SUPPLEMENT SERIES

*Astron. Astrophys. Suppl. Ser.* **119,** 439-457 (1996)



# IRAS sources beyond the solar circle. VII. The $^{12}C/^{13}C$ ratio in the far outer Galaxy

J.G.A. Wouterloot[1] and J. Brand[2]

[1] I. Physikalisches Institut, Zülpicher Strasse 77, D 50937 Köln, Germany
[2] Istituto di Radioastronomia, CNR, Via Gobetti 101, I 40129 Bologna, Italy

Received October 20, 1995; accepted February 24, 1996

**Abstract.** — We have investigated the $^{12}C/^{13}C$ abundance ratio in the far-outer Galaxy. We have used the IRAM 30-m telescope to obtain the $^{12}CO$ and $^{13}CO(1-0)$ and $(2-1)$ distributions towards five IRAS sources at about 16−17 kpc from the galactic center. $C^{18}O(1-0)$ and $(2-1)$ were observed towards the $^{13}CO$ peak positions in those clouds. The source with the strongest $C^{18}O$ emission, WB 89-437, was subsequently observed in $^{13}C^{18}O(1-0)$ and $(2-1)$ and in $H_2CS(3_{1,2}-2_{1,1})$ and $(6_{1,5}-5_{1,4})$. To be able to compare our results with published data, we observed the same transitions towards the inner Galaxy source W 33, and towards W 3OH. The ratio of the $^{13}CO$ and $C^{18}O$ column densities is about 14, slightly larger than what was found in local GMCs. This ratio is dominated by excitation and beam filling effects, and is therefore not indicative of the abundance ratios. The ratio $C^{18}O(1-0)/^{13}C^{18}O(1-0)$ directly yields the $^{12}C/^{13}C$ abundance ratio however, for which towards WB 89-437 we find a $3\sigma$ lower limit of 201±15, which means that the $^{12}C/^{13}C$ gradient found in the inner Galaxy continues further out. Our results for W 33 and W 3OH are consistent with earlier observations and give abundance ratios of 43.0±4.3 and 85±15, respectively. These $J$=1−0 measurements are however in contrast to results obtained from the corresponding $J$=2−1 transitions: we obtain abundance ratios of 104±60 (WB 89-437), 31±2 (W 33), and 24±2 (W 3OH). These differences may be due to the emission of the two transitions originating in different parts of the cloud with different excitation conditions. The $^{12}CO$ emission towards WB 89-437 shows strong outflow emission, and that of WB 89-380 is dominated by self-absorption. The sizes of the $^{13}CO$ clumps are 1−2 pc and they have peak positions located within 10″ (0.5 pc) from the IRAS position. Their (virial) masses are typically several 1000 $M_\odot$.

**Key words:** ISM: abundances — ISM: molecules — Galaxy: abundances — radio lines: ISM

## 1. Introduction

One of the aims in the study of molecular clouds, is the determination of their column densities and masses. Combining data of $^{12}CO(1-0)$ and $^{13}CO(1-0)$, LTE-column densities can be calculated assuming that the excitation temperatures of both molecules are equal and adopting some value for the $^{13}CO$ abundance. Mass determinations in this way have been made only for clouds that are either nearby, and/or in the inner Galaxy using abundances derived from comparisons of molecular and optical data of local (solar neighbourhood) clouds and HII regions. From only $^{12}CO$- data, one can derive so-called "$W_{CO}$ column densities" $[W_{CO}=\int T_R^*(^{12}CO)dV]$, using an empirical value for the ratio $X=N_{H_2}/W_{CO}$, which has been found to lie in a relatively narrow range for many clouds, although its actual value is still under discussion (Wolfendale 1991).

Wouterloot & Brand (1989; hereafter WB 89) used the SEST and the IRAM 30-m telescope to make an extensive CO survey towards IRAS point sources located in the outer Galaxy (second and third quadrants), with infrared colours that discriminate in favour of sources frequently associated with $H_2O$ masers and dense molecular cloud cores (Wouterloot & Walmsley 1986). Subsequently, about 30 clouds located in the far-outer Galaxy (FOG; $R$>16 kpc, assuming $R_\odot$=8.5 kpc) were mapped in $^{12}CO(1-0)$ using the SEST and the 3-m KOSMA telescope (Brand & Wouterloot 1994). Two of these clouds were also mapped in $^{13}CO(1-0)$ and in other clouds $^{13}CO(1-0)$ was observed only at some positions.

Using these data, Brand & Wouterloot (1995) compared column densities $N_{Wco}$, derived adopting $X$=2.3 $10^{20}$ cm$^{-2}$(Kkm s$^{-1}$)$^{-1}$, with LTE column densities, $N_{lte}$. They showed that the LTE column densities are lower by a factor 5 than the ones, derived from the integrated $^{12}CO$ emission alone. This could indicate that

*Send offprint requests to*: J.G.A. Wouterloot

in the FOG $X$ is lower than the value used, which would however be in contradiction with other results indicating that $X$ should be higher in the far outer Galaxy. Alternatively the $^{13}$CO abundance in the FOG could be lower than the value which was assumed ($2\ 10^{-6}$, derived by Dickman (1978) for local clouds). This would agree with observational evidence of a gradient in the $^{12}$C/$^{13}$C ratio across the Galaxy (see Fig. 1 of Wilson & Matteucci 1992 (WM 92), and Wilson & Rood 1994). WM 92 combined data from Gardner & Whiteoak (1979), Henkel et al. (1980, 1982, 1985), and Langer & Penzias (1990). This ratio increases from about 40 at $R$=4.5 kpc to 80 at $R$=10.5 kpc, but has a large scatter. An extrapolation of the WM 92 fit to those data (an increase of the ratio of 6.2±1.6 kpc$^{-1}$) gives a $^{12}$C/$^{13}$C ratio of about 123 at $R$=16−20 kpc, the interval where the clouds from our present sample are located. According to their modeled gradient, the ratio would be about 110 in the FOG. Combined with the modeled gradient in $^{12}$C/H (for which there are no observational data yet), this would result in a ratio $N(^{13}\mathrm{CO})/N(\mathrm{H_2})$ of $3\ 10^{-7}$. Applying this value Brand & Wouterloot (1995) obtained column densities $N_{\rm lte}$ that are approximately equal to $N_{\rm Wco}$. Beyond $R$=12 kpc there are very few observational data on abundances, however. Fich & Silkey (1991) derived the abundances of several elements from observations of optically visible HII regions at $R$=11.5−17.9 kpc, and found that, at least for nitrogen, the abundance gradient appears to be flatter in the FOG with respect to the extrapolation of the gradient found by Shaver et al. (1983) for $R\leq$12 kpc. Rolleston et al. (1994) obtained abundances from measurements of stars at $R$=13 kpc, and found a large scatter with some values close to those in the solar neighbourhood. However it is possible that such stellar abundances do not reflect the true ones because of mixing processes. Recently, Rudolph et al. (1994) concluded from observations of far-infrared fine structure lines of N, O, and S towards compact HII regions, that there is an abundance gradient continuing beyond 15 kpc from the galactic center. Also in external galaxies there is no indication for flattening of abundance gradients (see Henry & Howard 1995).

To investigate whether the relevant abundance gradients really continue beyond distances from the galactic centre, $R$, larger than 11 kpc, we have used the IRAM 30-m telescope to observe 5 clumps associated with IRAS sources with 16<$R$<17 kpc, in several CO isotopes. One of these clumps was observed in $^{13}$C$^{18}$O(1−0) and (2−1), and combining those data with C$^{18}$O(1−0) and (2−1), we can obtain information on the $^{12}$C/$^{13}$C ratio in that cloud, similar to the observations of Wannier et al. (1976), Wilson et al. (1981) and Langer & Penzias (1990, 1993) for several inner Galaxy and solar neighbourhood clouds. The observational method is described in Sect. 2, the results are shown in Sect. 3, and abundance ratios are derived and discussed in Sect. 4.

## 2. Observations

From WB 89 we have selected 5 sources (listed in Table 1), which have $T[^{12}\mathrm{CO}(1-0)]$>10 K when observed with the IRAM 30-m telescope. Because the $^{12}$CO and $^{13}$CO emission towards such sources peak close to, but not at the IRAS position (which has an uncertainty of 10″−30″), we mapped on May 1-3, 1993 with the IRAM 30-m telescope a small region around each source simultaneously in $^{12}$CO(2−1), $^{13}$CO(1−0), and $^{13}$CO(2−1), using three SIS receivers. The beam size of the 30-m telescope is about 22″ for the (1−0) transitions and about 11″ for the (2−1) transitions, which at the distances of the sources corresponds to resolutions of 0.92−1.12 pc and 0.46−0.56 pc, respectively. We first observed the regions on a 24″ raster and then zoomed in around the $^{13}$CO peaks using a 12″ raster or an (incomplete) 6″ raster. To obtain information about the CO excitation we also observed $^{12}$CO(1−0) at some positions in the cloud centers. As backends we used a 128-channel filterbank with a resolution of 100 kHz [for $^{13}$CO(2−1)], and an autocorrelator split into three parts with 1792 channels each with resolutions of 39 kHz [for $^{13}$CO(1−0), $^{12}$CO(1−0), and $^{12}$CO(2−1)]. All observations were done in total power mode with reference positions (see Table 1) chosen using the maps from Brand & Wouterloot (1994). Typical rms noise values in the maps are 0.10 −0.15 K [$^{13}$CO(1−0, 2−1)], and 0.3−0.4 K [$^{12}$CO(1−0, 2−1)]. In Table 1, Col. 1 gives the source number from WB 89 and Col. 2 the IRAS name. The positions in galactic coordinates (given in Cols. 3 and 4) deviate slightly from the IRAS positions due to a small error in the conversion program. In Col. 5 we therefore list the offset of the IRAS source with respect to the center position used. Columns 6-8 give the distances from the Sun and the galactic centre, and the luminosity of the IRAS source. The reference position used is given in Col. 9.

Because $^{13}$CO is much less optically thick than $^{12}$CO, its emission can be used to trace the position with the highest column density. Towards the positions of the $^{13}$CO peaks near the five sources in Table 1, we have measured C$^{18}$O(1−0) and (2−1) on October 7-10, 1993 (however few data were obtained due to bad weather, and all spectra were discarded) and September 18-22, 1994. In order to check whether these observations are consistent with the maps, we simultaneously also observed $^{13}$CO(1−0), and $^{12}$CO(2−1). For these observations we used an autocorrelator split into 4 parts with 448 channels [39 kHz resolution; C$^{18}$O(1−0) and $^{13}$CO(1−0)], 897 channels [78 kHz resolution; C$^{18}$O(2−1)], and 1345 channels [78 kHz resolution; $^{12}$CO(2−1)] respectively. In the same transitions we mapped a small region on a 24″ raster around the centre of the $^{13}$CO(2−1) map of W 33 by Goldsmith & Mao (1983) [(0″,0″) is at $\alpha(1950)=18^{\rm h}\ 11^{\rm m}\ 19^{\rm s}$, $\delta(1950)=-17^\circ 56'\ 46''$]. The rms noise levels towards the FOG sources are typically 0.020 K [C$^{18}$O(1−0) and $^{13}$CO(1−0)], 0.023 K [C$^{18}$O(2−1)], and 0.025 K [$^{12}$CO(2−1)]. In the W 33 map

**Table 1.** Observed sources

| WB89 | IRAS | $l$ | $b$ | IRAS offset $''$ | $d$ kpc | $R$ kpc | $L_{\rm fir}$ $L_\odot$ | Ref. pos. $''$ |
|---|---|---|---|---|---|---|---|---|
| 380 | IRAS01045+6505 | 124.6471 | 2.5399 | (−16,−4) | 10.43 | 16.77 | 1.0 $10^5$ | (0,1000) |
| 391 | IRAS01160+6529 | 125.8070 | 3.0499 | (−9,−11) | 10.49 | 16.91 | 1.0 $10^4$ | (0,1000) |
| 399 | IRAS01420+6401 | 128.7770 | 2.0098 | (−3,10) | 9.94 | 16.63 | 4.2 $10^4$ | (−1000,0) |
| 437 | IRAS02395+6244 | 135.2772 | 2.7999 | (2,−10) | 9.07 | 16.24 | 7.1 $10^4$ | (1000,0) |
| 501 | IRAS03483+5739 | 145.1970 | 2.9899 | (−4,−12) | 8.59 | 16.30 | 8.9 $10^3$ | (1000,0) |

these values are 0.25 K [$C^{18}O(1-0, 2-1)$], and 0.3−0.5 K [$^{13}CO(1-0)$ and $^{12}CO(2-1)$].

Towards WB 89-437, the FOG source with the strongest $C^{18}O(1-0)$ emission, we used the 3-mm SIS receiver during the run of September 18-22, 1994 to search for $^{13}C^{18}O(1-0)$ emission at 104.711383 GHz. To check the receiver tuning, we simultaneously observed the $H_2CS$ ($3_{1,2}-2_{1,1}$) line at 104.616977 GHz, which is expected to be stronger than $^{13}C^{18}O(1-0)$, and with the two 1.3-mm SIS receivers we observed $C^{18}O(2-1)$ and $^{13}CO(2-1)$ or $^{12}CO(2-1)$ in order to monitor the pointing of the telescope by comparing the line intensities with those previously found. Towards W 33 we observed $^{13}C^{18}O(1-0)$ at the $C^{18}O(1-0)$ peak, and observed towards the mapped positions with shorter integration times in order to compare our $^{13}C^{18}O(1-0)$ data with the lower resolution measurements of Langer & Penzias (1990). During these observations we used the autocorrelator split into 5 parts with 448 channels [39 kHz resolution; $H_2CS$ ($3_{1,2}-2_{1,1}$) and $^{13}C^{18}O(1-0)$], 225 channels [312.5 kHz resolution; $^{13}C^{18}O(1-0)$], 897 channels [78 kHz resolution; $C^{18}O(2-1)$], and 1345 channels [78 kHz resolution; $^{12}CO(2-1)$ or $^{13}CO(2-1)$] respectively.

Reducing the September 1994 data we found that $C^{18}O(2-1)$ generally is much stronger than $C^{18}O(1-0)$, and on August 15-20, 1995 we have observed the $^{13}C^{18}O(2-1)$ transition at 209.419141 GHz, together with $H_2CS$ ($6_{1,5}-5_{1,4}$) at 209.200141 GHz. In addition we simultaneously observed again the $^{13}C^{18}O(1-0)$, $H_2CS$ ($3_{1,2}-2_{1,1}$) and $C^{18}O(2-1)$ in the same way as in September 1994. The receiver used to observe $C^{18}O(2-1)$ was frequently instable, and the data are not usable. The autocorrelator set-up for $^{13}C^{18}O(1-0)$ and $H_2CS$ ($3_{1,2}-2_{1,1}$) was the same as in September 1994. For $^{13}C^{18}O(2-1)$ we used 449 channels (78 kHz resolution) and 225 channels (312.5 kHz resolution), and for $H_2CS$ ($3_{1,2}-2_{1,1}$) 449 channels (78 kHz resolution).

During all observations, pointing was regularly checked on the nearby sources NGC 7538 or W 3OH and was found to have rms accuracies in azimuth and elevation of about $4''$ (May 1993) and $2''$ (September 1994, August 1995). Line intensities were checked on W 3OH ($\alpha(1950)=2^{\rm h}\ 23^{\rm m}\ 16.5^{\rm s}$, $\delta(1950)=61°38'\ 57''$) [using a reference position at ($7200''$, $0''$)] and are comparable to those in Mauersberger et al. (1989) (for transitions also observed by these authors). We detected emission towards the reference position at ($-3600''$, $0''$), which was also used by Mauersberger et al., and it should therefore be avoided. Their $C^{18}O(1-0)$ spectrum has probably been calibrated wrongly (Mauersberger, private communication), because we always found line intensities of 2.5−2.7 K (compared to a Mauersberger et al. value of 4.6 K). Because all cloud emission is more extended than the main beam sizes of $11'' - 22''$, all line intensities in the present paper are in units of $T_{\rm A}^*$ ($B_{\rm eff}$=$F_{\rm eff}$; see Downes (1989) for a discussion of efficiencies adopted at the 30-m telescope), with forward efficiencies $F_{\rm eff}$ values of 0.86 (May 1993) and 0.92 (September 1994, August 1995) at 3-mm, and of 0.76 (May 1993) and 0.86 (September 1994, August 1995) at 1.3-mm. The values for $B_{\rm eff}$ are 0.68 (3-mm) and 0.40 (1.3-mm).

## 3. Results

The distribution of $^{12}CO$ and $^{13}CO$ (1−0) and (2−1) emission towards the five WB 89 sources is shown in Figs. 1a-e. Within each cloud we observed the $^{13}CO$ peak position in $C^{18}O$. These positions are listed in Col. 2 of Table 2. Column 3 gives the offset (in galactic coordinates) of this position from the IRAS position (see Col. 5 of Table 1). From contour plots (not shown) of the integrated $^{13}CO(1-0)$ and (2−1) emission we have estimated the size of the clumps associated with the IRAS sources. We determined the size of the minor and major axis at the half power level, and corrected for the angular resolution. These sizes are listed in arcsec in Cols. 4 [$^{13}CO(1-0)$] and 5 [$^{13}CO(2-1)$] of Table 2, and in pc in Col. 6, using the distances of the sources given in Table 1. Using the cloud-averaged $^{13}CO(1-0)$ line widths $\delta v$ in Col. 7 of Table 2 we derived the virial masses in Col. 8, assuming gaussian clumps ($M_{\rm vir}$=370d$\delta v^2 \tan\sqrt{A_{1/2}/\pi}$), where $A_{1/2}$ is the cloud area at the half power level.

The spectra observed towards the $^{13}CO$ peak positions are shown for the five sources in Fig. 2 [$^{12}CO$ and $^{13}CO$ (1−0, 2−1)] and in Fig. 3 [$C^{18}O(1-0, 2-1)$].

### 3.1. *W 33*

The $^{13}CO(2-1)$ map of W 33 by Goldsmith & Mao (1983) was made with a resolution of about $1'.6$ (≈1.9 pc at a

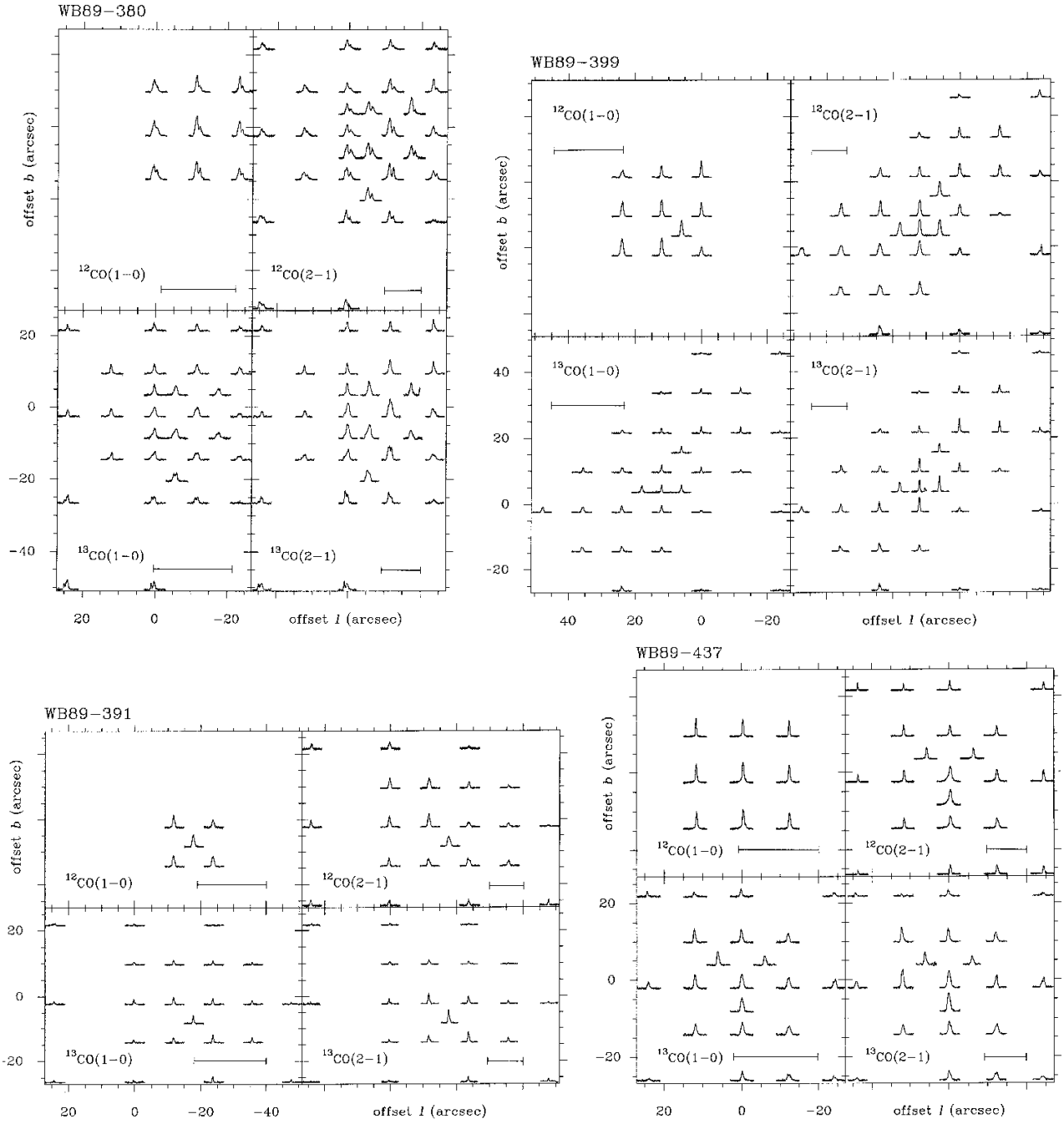


**Fig. 1.** Distribution of $^{12}$CO(1−0) and (2−1) and $^{13}$CO(1−0) and (2−1) emission towards five FOG IRAS sources. Offsets are in arcseconds with respect to the positions given in Table 1. Below we give the velocity and $T_{\rm A}^{*}$ ranges for the sources. The velocity ranges are equal for $^{12}$CO and $^{13}$CO, except for WB89-437 because of the strong $^{12}$CO outflow. The horizontal bars indicate the half power beam width. **a)** WB 89-380; −95 to −75 km s$^{-1}$; −2 to 20 K ($^{12}$CO); −0.5 to 6 K ($^{13}$CO). **b)** WB 89-391; −95 to −75 km s$^{-1}$; −2 to 18 K ($^{12}$CO); −1 to 7.5 K ($^{13}$CO). **c)** WB 89-399; −92 to −72 km s$^{-1}$; −2 to 20 K ($^{12}$CO); −1 to 8 K ($^{13}$CO). **d)** WB 89-437; −100 to −50 km s$^{-1}$; −2 to 20 K ($^{12}$CO); −82 to −62 km s$^{-1}$; −1 to 6 K ($^{13}$CO). **e)** WB 89-501; −69 to −49 km s$^{-1}$; −2 to 25 K ($^{12}$CO); −1 to 8 K ($^{13}$CO)

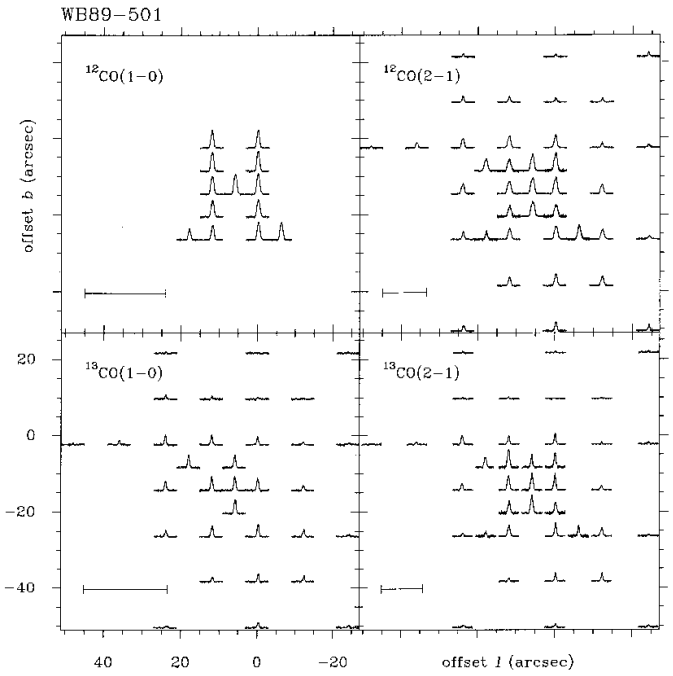


**Fig. 1.** continued

**Table 2.** Clump parameters

| WB 89 | $^{13}$CO peak $''$ | offset from IRAS $''$ | $^{13}$CO(1−0) size $''$ | $^{13}$CO(2−1) size $''$ | size pc | $^{13}$CO(1−0) $\delta v$ km s$^{-1}$ | $M_{\rm vir}$ $M_\odot$ |
|---|---|---|---|---|---|---|---|
| 380 | (−12,0) | (4,4) | 23x45 | 17x45 | 0.86x2.28 | 3.51 | 3600 |
| 391 | (−18,−6) | (−9,5) | 18x37 | 15x28 | 0.76x1.42 | 1.48 | 480 |
| 399 | (6,6) | (9,−4) | 33 | 17x61 | 0.82x2.94 | 2.06 | 1380 |
| 437 | (0,0) | (−2,10) | 31x40 | 15x36 | 0.66x1.58 | 2.73 | 1590 |
| 501 | (6,−12) | (10,0) | 19x36 | 19x19 | 0.79x0.79 | 2.02 | 670 |

distance of 4 kpc). It shows a maximum at (0,0), corresponding to the radio continuum source G12.8−0.2 (Goss et al. 1978). Following Goldsmith & Mao, we used a reference position at (−1800″, 0″). Checking this against a reference position at (1800″, 0″), we see faint (about 0.5 K) emission in $^{13}$CO(1−0) at 30 km s$^{-1}$ (and (1800″,0″) shows 1 K emission at 39 km s$^{-1}$), but none (<0.1 K) in C$^{18}$O(1−0). In $^{12}$CO(2−1) there is confusion because both reference positions contain lines of about 0.5−2 K at velocities between 11 and 51 km s$^{-1}$. In addition there is weaker emission between 62 and 77 km s$^{-1}$ at (−1800″,0″). This does however not affect our conclusions. The spectra of the maps made towards W 33 are shown in Fig. 4. The $^{12}$CO emission is very complex, with large variations within the 24″ grid. However only one of the components contains high density gas as shown by the single component at 35 km s$^{-1}$ seen in C$^{18}$O, which is strongly peaked near a compact core in the northern part of the radio continuum source (see the 6 cm map by Ho et al. 1986). The C$^{18}$O(1−0) clump size at half maximum is 85″×59″, or 1.6×1.1 pc$^2$, which is slightly larger than the radio continuum source. With a cloud-averaged line width of 5.35 km s$^{-1}$, the virial mass of this clump would be 8200 $M_\odot$. From the maps in Fig. 4 we chose the offset position (0″, 24″) (where is the $\int T(\mathrm{C^{18}O})\mathrm{d}v$ peak) to be observed with longer integration time in $^{13}$C$^{18}$O because it would be less affected by pointing errors than e.g. (0″, 48″) because of the steep gradient north of the latter position.

### **3**.2. *WB 89-380*

This is the most luminous source from the sample. The $^{12}$CO emission shows strong self-absorption (see Fig. 2), the $^{13}$CO and C$^{18}$O emission being at the velocity of the $^{12}$CO dip. Also the $^{13}$CO spectra show two peaks, but in this case it is probably caused by the presence of two velocity components at about −85.5 and −87 to −88 km s$^{-1}$. These are also seen in C$^{18}$O as an asymmetric line profile. Wouterloot et al. (1993) found $H_2O$ maser

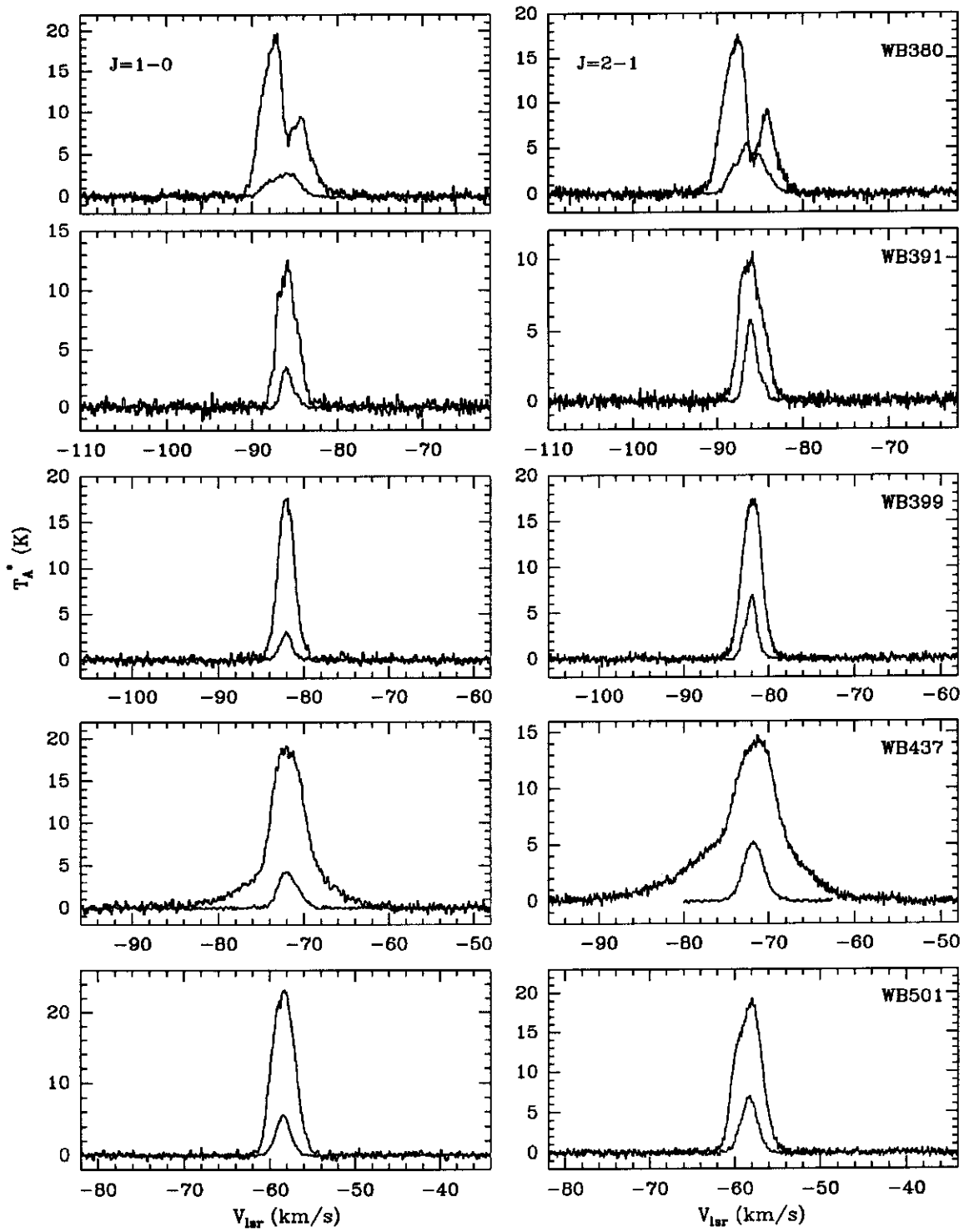


**Fig. 2.** $^{12}$CO and $^{13}$CO spectra at the five $^{13}$CO peak positions for the (1−0) (left) and (2−1) (right) transitions. All spectra are on the same (relative) velocity scale

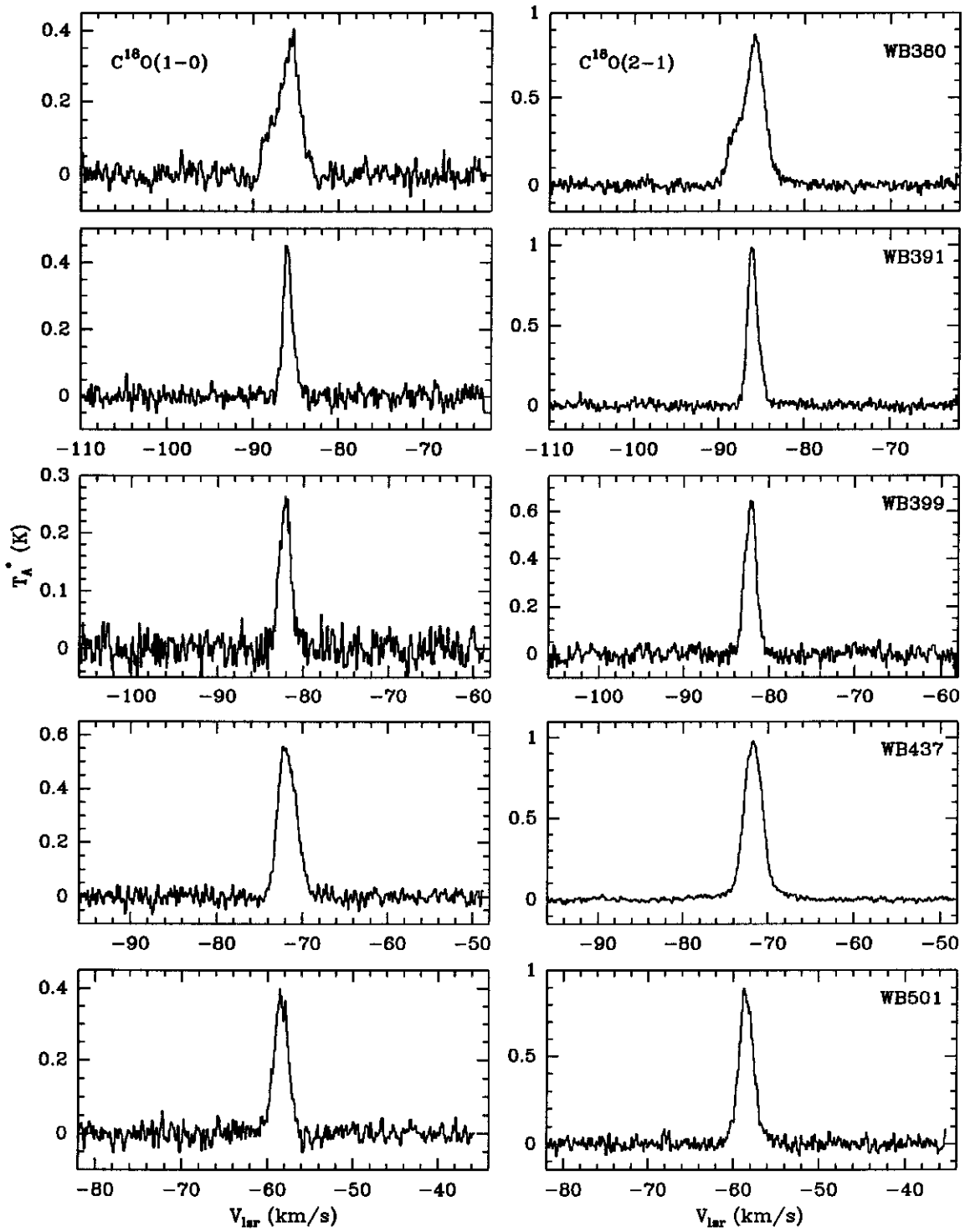


**Fig. 3.** $C^{18}O(1-0)$ (left) and $C^{18}O(2-1)$ (right) spectra towards the five $^{13}CO$ peak positions. All spectra are on the same (relative) velocity scale

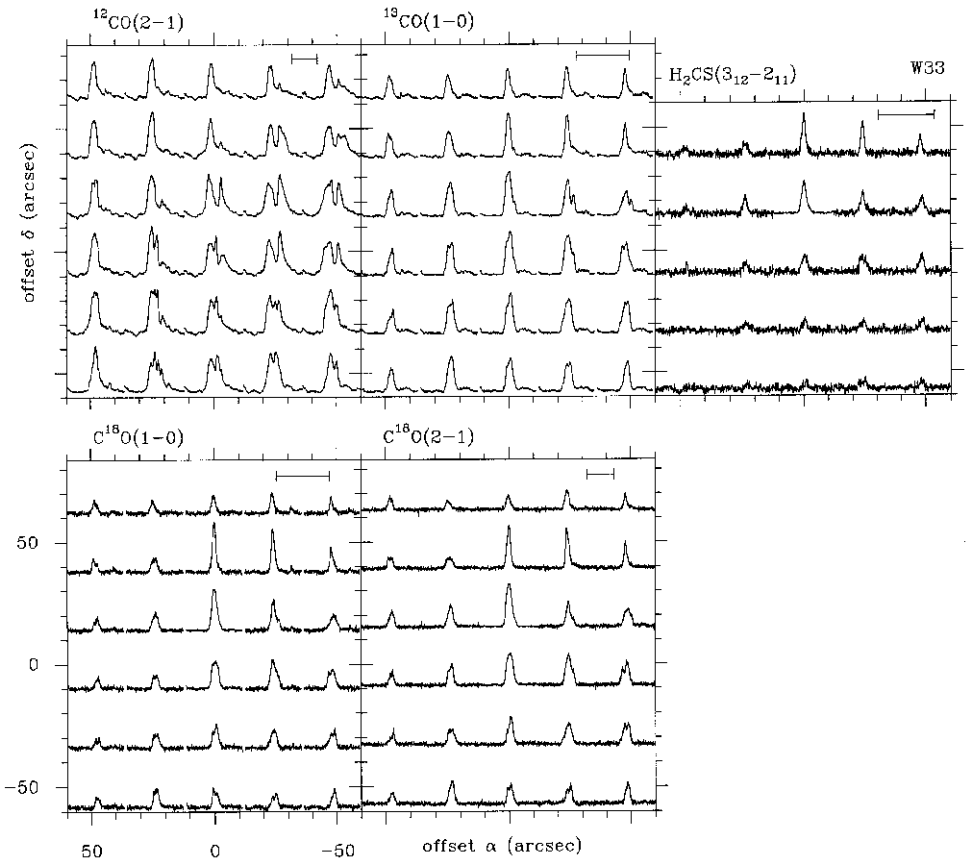


**Fig. 4.** Spectra towards W33. The velocity range is 10 to 60 km s$^{-1}$, and the $T_{\rm A}^{*}$ ranges are −3 to 27 K [$^{12}$CO(2−1) and $^{13}$CO(1−0)], −1 to 11 K [C$^{18}$O(1−0)], −2 to 13 K [C$^{18}$O(2−1)], and −0.3 to 2.2 K [H$_2$CS(3$_{1,2}$−2$_{1,1}$)]. Offsets are in arcseconds with respect to $\alpha$(1950)=18$^{\rm h}$ 11$^{\rm m}$ 19$^{\rm s}$, $\delta$(1950)=−17°56′ 46″. The horizontal bars indicate the half power beam width

emission towards this source. The maser position corresponds to an offset of (−11″, 2″) in our map and of (1″, 2″) with respect to the $^{13}$CO peak. Rudolph et al. (1996) detected a compact HII region associated with the IRAS source at offset (−12″, −3″) in our map and of (0″, −3″) with respect to the $^{13}$CO peak. The cloud was observed with the BIMA interferometer in CS(2−1) and in $^{12}$CO(1−0) by de Geus et al. (1996). A CS peak coincides with the radio continuum source.

### **3**.3. *WB 89-391*

This source shows the narrowest C$^{18}$O emission (though slightly asymmetric) with line widths of about 1.4 km s$^{-1}$, and there is no significant velocity gradient within the clump. The $^{12}$CO(2−1) emission near the $^{13}$CO peak is probably affected by self-absorption. Rudolph et al. (1996) detected a radio continuum point source (size 2.″9) towards offset (0″, −8″).

### **3**.4. *WB 89-399*

The distribution of the $^{13}$CO emission is elongated and shows several maxima in the (2−1) transition. In the lower left corner of the map there are two velocity components at −82.2 km s$^{-1}$ and at about −81 km s$^{-1}$. Therefore the size of this cloud is not well-defined and we give only one approximate number for $^{13}$CO(1−0). Rudolph et al. (1996) detected an extended radio continuum source at 6 cm (size 20″) towards offset (−1″, 9″). It is coincident with an optically visible nebula of the same size.

### **3**.5. *WB 89-437*

Although the luminosity of this source (IRAS02395+6244; RAFGL 5077) is 7.1 10$^4$ $L_\odot$ (i.e. a single O8V$_0$ star; Panagia 1973), Rudolph et al. (1996) found no radio continuum emission stronger than 0.18 mJy at 6 cm. This suggests that the source is very young. The H$_2$O maser found by Wouterloot et al. (1993) is at offset (7″, −14″). The cloud was observed with the BIMA interferometer in CS(2−1) and in $^{12}$CO(1−0) by de Geus et al. (1996). A CS clump was found at offset (2″, −7″), the size

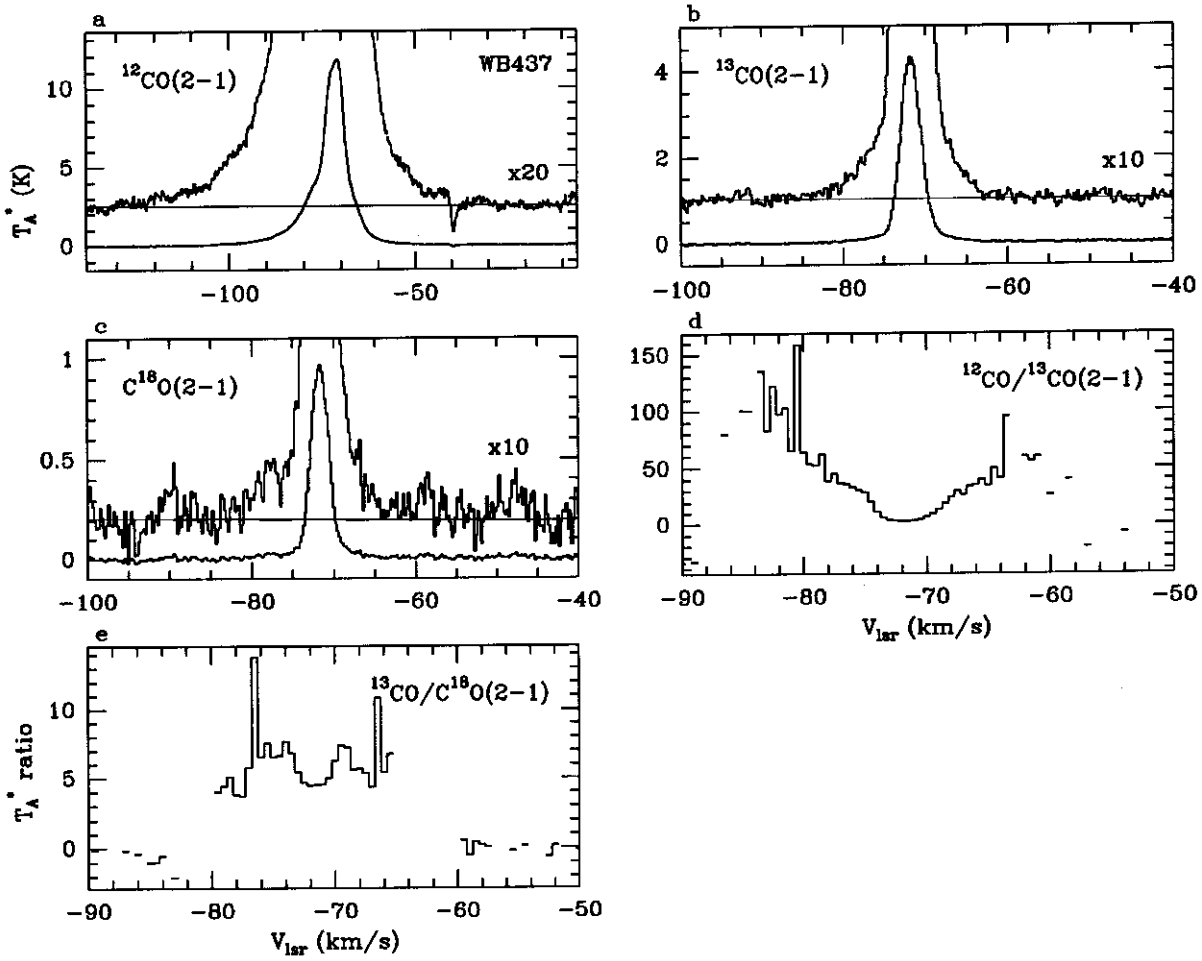


**Fig. 5. a-c)** Deep $^{12}$CO(2−1), $^{13}$CO(2−1), and C$^{18}$O(2−1) spectra of the outflow emission towards WB 89-437 at offset (0″, 0″), resampled to 0.2 km s$^{-1}$ resolution. **d)** The ratio of the $^{12}$CO(2−1) and $^{13}$CO(2−1) $T_A^*$ (velocity resolution 0.5 km s$^{-1}$). **e)** The ratio of the $^{13}$CO(2−1) and C$^{18}$O(2−1) $T_A^*$ (velocity resolution 0.5 km s$^{-1}$)

(1.35 pc) of which is close to that which we derive for the clump found in $^{13}$CO(2−1) (see Table 2). The $^{12}$CO(2−1) spectrum towards (0″, 0″) shows strong emission in the line wings. A spectrum obtained simultaneously with our $^{13}$C$^{18}$O data (see Sect. 4.2), is shown in Fig. 5a. The rms is 10 mK (at a velocity resolution of 0.2 km s$^{-1}$), and shows emission from −120 to −40 km s$^{-1}$ (a first order baseline was subtracted using the velocity interval outside −125 to −20 km s$^{-1}$). The spectrum shows a line of −0.1 K at −40 km s$^{-1}$, which is probably due to emission in the reference position [at (1000″, 0″)] from a very optically thin foreground cloud (though possibly also the source position contains emission at this velocity). The outflow is weaker in $^{12}$CO(1−0) than in $^{12}$CO(2−1) (see Fig. 2), because of beam dilution: convolving the (2−1) map to the (1−0) resolution (not shown), the outflow emission is equally strong in both transitions, whereas the quiescent emission is stronger in (1−0). The distribution of the outflow is compared with that of the quiescent ($^{12}$CO and $^{13}$CO) gas in Fig. 6. The extent of the blue wing (Fig. 6c) is less than 12″ (0.5 pc), whereas the red wing (Fig. 6d) is somewhat more extended and its centre is displaced from that of the blue outflow and the quiescent gas. Because of these small sizes, parameters like energy, momentum and dynamical age, should be derived from higher resolution data. The $^{13}$CO(2−1) spectra suggest that there are two velocity components in the cloud, at about −70 km s$^{-1}$ and at −72 km s$^{-1}$. In Figs. 5b and c we show the $^{13}$CO(2−1) and C$^{18}$O(2−1) spectra which were observed simultaneously with the $^{13}$C$^{18}$O(1−0). The rms in the spectra is 7 mK ($^{13}$CO) and 6 mK (C$^{18}$O) and they show weak outflow emission. The spectrum of the ratio of $^{12}$CO(2−1) and $^{13}$CO(2−1) emission (stronger than 7 mK) is shown in Fig. 5d. The ratio in the line center is 2.75, and increases to more than 100 in the blue line wing, indicating that the $^{12}$CO emission at those extreme velocities is very optically thin. The ratio is consistent with the ratio derived from the C$^{18}$O(2−1) and $^{13}$C$^{18}$O(2−1)

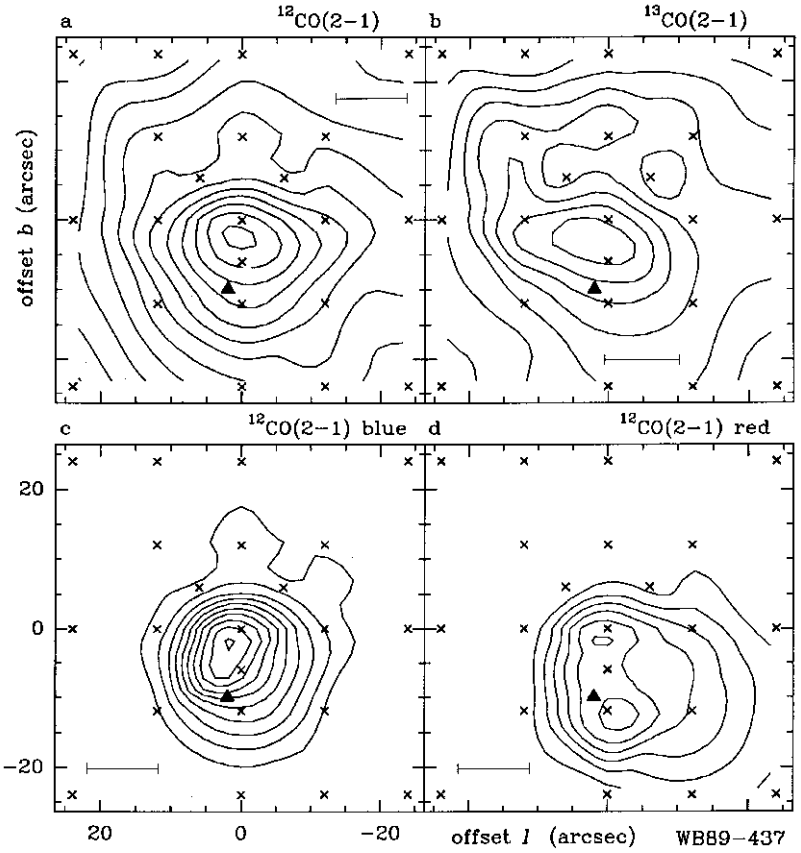


**Fig. 6.** The WB 89-437 cloud. The position of IRAS 02395+6244 is indicated by the filled triangle. Offsets (in galactic longitude and latitude) are in arcseconds with respect to (135.2772, 2.7999). The horizontal bars indicate the half power beam width. **a)** Quiescent $^{12}$CO(2−1) emission with $V_{\rm lsr}$ −74 to −69 km s$^{-1}$. Contour levels are 10 (5) 65 Kkm s$^{-1}$. **b)** Quiescent $^{13}$CO(2−1) emission with $V_{\rm lsr}$ −74 to −69 km s$^{-1}$. Contour levels are 3 (2) 15 Kkm s$^{-1}$. **c)** Blue wing emission with $V_{\rm lsr}$ −90 to −76 km s$^{-1}$. The contour levels are 3 (3) 27 Kkm s$^{-1}$. **d)** Red wing emission with $V_{\rm lsr}$ −68 to −55 km s$^{-1}$. The contour levels are 3 (3) 18 Kkm s$^{-1}$

emission (see Sect. 4.2). Similar observations have been made towards outflows in NGC 2071, S 140, and Orion by Snell et al. (1984). Located at smaller distances from the galactic center than WB 89-437, those sources show ratios in the line wings between 20 and 80. From the average $^{12}$CO(2−1)/$^{13}$CO(2−1) ratios of the WB 89-437 outflows, 54.5 (blue) and 27.5 (red), and assuming a $^{12}$C/$^{13}$C abundance ratio of 150, the average $^{12}$CO(2−1) optical depths are 2.5 (blue), and 5.5 (red). The spectrum of the $^{13}$CO/C$^{18}$O(2−1) ratio shows a minimum of 4.5 at the peak velocity and a slightly increasing value at other velocities, probably also caused by optical depth effects in $^{13}$CO(2−1). This increase towards the linewings of this ratio is found more significantly in the (1−0) spectra (towards W 3OH, DR 21OH, OriA, and W 33) by Langer & Penzias (1990). They suggest that another explanation may be that this wing emission originates in regions affected by fractionation.

### 3.6. *WB 89-501*

From gaussian fits to the $^{13}$CO(2−1) spectra we find that there is a velocity gradient from approximately −57.8 km s$^{-1}$ in the lower right corner to −58.8 km s$^{-1}$ in the upper left corner of our map. A near infrared H CCD-frame, made at UKIRT, shows two about equally bright embedded objects, possibly in addition to several much weaker ones.

## 4. Isotopic ratios

### 4.1. *The ratio* $^{13}$CO/C$^{18}$O

The intrinsic abundance ratio $^{13}$CO/C$^{18}$O is not expected to change significantly with $R$: the gradients in $^{12}$C/$^{13}$C and $^{16}$O/$^{18}$O for the range 3.5<$R$<10.5 kpc almost cancel. The local ratio $^{13}$CO/C$^{18}$O, is 7. According to the modeled galactic abundance gradients listed by WM 92 in their Table 1, the value at $R$=17 kpc would be 7.5 and extrapolating average values for the observed gradients,

the ratio would be 8.3. Both numbers are very close to the local value and galactic differences are probably not observable.

However the measured ratios of the integrated line intensities of $^{13}$CO and C$^{18}$O may not represent the intrinsic ratio because of fractionation, optical depth and filling factor effects (Taylor & Dickman 1989; Langer & Penzias 1990). Since the clouds in the present sample are located at approximately equal distances from the Sun (10 kpc) we can compare our results with those towards local dark clouds and GMC's, which have an intrinsic ratio of 7-8 (WM 92), and with the solar system ratio of 5.5.

In Table 3 we list line parameters derived from the $^{12}$CO, $^{13}$CO and C$^{18}$O (1−0) and (2−1) spectra towards the $^{13}$CO peak positions in the FOG sources where we observed both C$^{18}$O transitions. Because some sources have a non-gaussian line profile (WB 89-380, 391, and 437), we give in Col. 5 for all sources the weighted average velocity of the emission (first moment) rather than a value obtained from gaussian fits. The line width in Col. 6 is the width at half maximum, read from the spectra. For $^{13}$CO(1−0) we give two results. The first (indicated with 'a' in Col. 7) was obtained simultaneously with the $^{13}$CO(2−1) emission, whereas the second one ('b') was observed simultaneously with both C$^{18}$O lines. Differences between both $^{13}$CO(1−0) results might be due to pointing errors, which might have been slightly larger during the (1993) mapping observations ('a'; see Sect. 2).

From Table 3 we derived the ratios of the $^{13}$CO and C$^{18}$O line intensities for the (1−0) and (2−1) transitions, which are listed in Cols. 2 to 4 of Table 4. Both (1−0) transitions have been observed simultaneously and should be more accurate than the (2−1) ratios. To obtain the latter ratios we have scaled the $^{13}$CO(2−1) intensities with the ratio of $^{13}$CO(1−0) $T_{\rm A}^*$ obtained in measurements 'b' and 'a' (see Table 4). Only towards WB 89-437 both (2−1) transitions were observed simultaneously during the $^{13}$C$^{18}$O(1−0) observations. The median and average ratios of the integrated antenna temperatures of the (1−0) transition are 12.4 and 12.6 respectively. For the (2−1) transition these numbers are lower: 9.3 and 8.9. Assuming LTE conditions and using the excitation temperature derived from our $^{12}$CO(1−0) spectrum (Col. 6 of Table 4), we obtain the column densities from the (1−0) data listed in Col. 11 ($^{13}$CO) and Col. 12 (C$^{18}$O). Their ratio is given in Col. 13, and should be the abundance ratio in the clouds. The mean value is 13.9 (median 14.4), which is slightly larger than the ratios in Cols. 2 and 3 due to optical depth effects.

The $^{13}$CO and C$^{18}$O data towards the FOG sources were also analyzed using an escape probability model (Stutzki & Winnewisser 1985), which assumes a spherical cloud with constant density and kinetic temperature $T_{\rm kin}$. For $T_{\rm kin}$ we first adopted the derived value for the $T_{\rm ex}$($^{12}$CO). In addition, because it has been suggested that $^{13}$CO and C$^{18}$O originate in colder regions in cloud interiors (see e.g. Castets et al. 1990 for the case of Orion) we adopted $T_{\rm kin}$ values 5 K (3 K for WB 89-391) lower than $T_{\rm ex}$ for $^{13}$CO and 10 K (6 K) lower for C$^{18}$O. For each value of $T_{\rm kin}$ we varied log$n_{\rm H_2}$ in steps of 0.25 between 2 and 5 and log[$N$(CO)/$\Delta v$] in steps of 0.25 between 14.0 and 18.8; here $n_{\rm H_2}$ is the H$_2$ volume density, and $N$(CO) the CO column density. Comparing the observed and modeled $^{13}$CO(2−1)/$^{13}$CO(1−0) ratios and peak $^{13}$CO(1−0) temperatures, the combination of $n_{\rm H_2}$ and $N/\Delta v$ with the lowest $\chi^2$ was obtained. To obtain the observed line ratios we convolved the $^{13}$CO(2−1) maps to the (1−0) resolution. Because we did not map the C$^{18}$O(2−1) distributions we adopted the correction factor resulting from the convolution of the $^{13}$CO(2−1) maps. The assumed values of $T_{\rm kin}$, and the resulting values of log$n_{\rm H_2}$ and $N$ (using the observed $^{13}$CO(1−0) and C$^{18}$O(1−0) line widths) are listed in Cols. 7 to 12 of Table 4, and the derived ratios of the column densities are in Col. 13. It is seen that the column densities from the escape probability model are smaller than the LTE values, which are listed on the first line in Cols. 11 and 12 for each object. However the ratios do not differ significantly, and there is also little dependence on the adopted kinetic temperatures: the average (median) ratios are 13.9 (13.3) and 13.6 (12.8) in the 'warm' and 'cold' case respectively.

We can compare our results with those of Taylor & Dickman (1989) for local dark clouds and giant molecular clouds. Plotting the $^{13}$CO/C$^{18}$O column density ratios versus $N$(C$^{18}$O) (corresponding to their Fig. 1), we find that the ratios towards the FOG clouds are slightly larger than found by Taylor & Dickman (1989) towards NGC 2264 at the same $N$(C$^{18}$O) (which are similar to those found in other GMCs), and are much larger than those found by Taylor & Dickman for local dark clouds. Taylor & Dickman argue that the differences in the ratios $N(^{13}{\rm CO})/N({\rm C}^{18}{\rm O})$ which they found between GMCs and dark clouds (and the solar system value) could be explained by larger filling factors for $^{13}$CO due to the presence of spatially unresolved clumps.

### 4.2. *The ratio* C$^{18}$O/$^{13}$C$^{18}$O

The observed line intensity ratio C$^{18}$O/$^{13}$C$^{18}$O is expected (Langer & Penzias 1990) to be close to the abundance ratio $^{12}$C/$^{13}$C with optical depth corrections for C$^{18}$O (the $^{13}$C$^{18}$O optical depth can be neglected) approximately cancelling the correction necessary because of the difference in frequency between the two observed transitions (see Linke et al. 1977):

$$\frac{\tau_{12}}{(1-{\rm e}^{-\tau_{12}})} \times \frac{\nu_{13}^2 {\rm e}^{-h\nu_{13}/kT_{\rm ex}}}{\nu_{12}^2 {\rm e}^{-h\nu_{12}/kT_{\rm ex}}} \qquad (1)$$

where 12 refers to $^{12}$C$^{18}$O and 13 to $^{13}$C$^{18}$O and $T_{\rm ex}$ is the LTE excitation temperature derived from $^{12}$CO. We used

**Table 3.** Line parameters FOG sources

| WB 89 | transition | $T_A^*$ K | | $\int T_A^* dV$ Kkm s$^{-1}$ | | $V_{lsr}$ km s$^{-1}$ | | $\delta v$ km s$^{-1}$ | | Remarks |
|---|---|---|---|---|---|---|---|---|---|---|
| 380 | $^{12}$CO(1-0) | 19.4 | 0.4 | 82.4 | 0.5 | −86.51 | 0.05 | 2.92 | 0.05 | sa |
| | | | | | | −87.2 | 0.05 | | | c |
| | $^{12}$CO(2-1) | 17.4 | 0.3 | 75.6 | 0.5 | −86.97 | 0.05 | - | | a,sa |
| | | | | | | −87.7 | 0.05 | | | c |
| | $^{13}$CO(1-0) | 3.60 | 0.02 | 14.73 | 0.08 | −86.30 | 0.01 | 4.24 | 0.10 | b |
| | | 2.77 | 0.12 | 11.16 | 0.40 | −86.44 | 0.07 | 4.38 | 0.10 | a |
| | $^{13}$CO(2-1) | 5.40 | 0.15 | 20.8 | 0.2 | −86.21 | 0.10 | 3.88 | 0.10 | a,sa |
| | C$^{18}$O(1-0) | 0.40 | 0.02 | 1.21 | 0.03 | −85.94 | 0.04 | 2.45 | 0.09 | b |
| | C$^{18}$O(2-1) | 0.86 | 0.02 | 2.79 | 0.02 | −86.08 | 0.01 | 2.64 | 0.05 | b |
| 391 | $^{12}$CO(1-0) | 12.2 | 0.4 | 34.5 | 0.5 | −85.92 | 0.04 | 2.84 | 0.05 | |
| | $^{12}$CO(2-1) | 10.3 | 0.3 | 33.5 | 0.5 | −85.97 | 0.03 | 3.27 | 0.05 | a |
| | $^{13}$CO(1-0) | 4.48 | 0.02 | 7.68 | 0.02 | −85.87 | 0.01 | 1.52 | 0.01 | b |
| | | 3.40 | 0.14 | 5.82 | 0.09 | −85.90 | 0.01 | 1.46 | 0.03 | a |
| | $^{13}$CO(2-1) | 5.65 | 0.13 | 10.34 | 0.07 | −85.90 | 0.01 | 1.52 | 0.01 | a |
| | C$^{18}$O(1-0) | 0.44 | 0.02 | 0.62 | 0.01 | −85.97 | 0.01 | 1.23 | 0.03 | b |
| | C$^{18}$O(2-1) | 0.97 | 0.02 | 1.47 | 0.01 | −85.88 | 0.01 | 1.37 | 0.02 | b |
| 399 | $^{12}$CO(1-0) | 17.7 | 0.3 | 43.4 | 0.5 | −82.07 | 0.01 | 2.26 | 0.02 | |
| | $^{12}$CO(2-1) | 17.4 | 0.3 | 49.4 | 0.1 | −81.96 | 0.01 | 2.62 | 0.01 | a |
| | $^{13}$CO(1-0) | 3.50 | 0.02 | 5.65 | 0.02 | −82.03 | 0.01 | 1.49 | 0.01 | b |
| | | 3.01 | 0.11 | 5.55 | 0.08 | −82.04 | 0.01 | 1.61 | 0.03 | a |
| | $^{13}$CO(2-1) | 6.70 | 0.10 | 11.06 | 0.07 | −82.09 | 0.01 | 1.50 | 0.01 | a |
| | C$^{18}$O(1-0) | 0.26 | 0.02 | 0.45 | 0.01 | −82.05 | 0.02 | 1.56 | 0.06 | b |
| | C$^{18}$O(2-1) | 0.65 | 0.02 | 1.10 | 0.01 | −82.08 | 0.01 | 1.62 | 0.02 | b |
| 437 | $^{12}$CO(1-0) | 19.1 | 0.3 | 113.5 | 0.5 | −72.20 | 0.05 | 4.50 | 0.05 | |
| | | | | | | −72.00 | 0.05 | | | c |
| | $^{12}$CO(2-1) | 14.4 | 0.2 | 128.7 | 0.5 | −72.93 | 0.05 | 6.14 | 0.05 | a |
| | | | | | | −71.20 | 0.05 | | | c |
| | $^{13}$CO(1-0) | 4.82 | 0.03 | 15.27 | 0.04 | −71.64 | 0.01 | 2.73 | 0.01 | b |
| | | 4.23 | 0.11 | 12.04 | 0.08 | −71.86 | 0.01 | 2.72 | 0.02 | a |
| | $^{13}$CO(2-1) | 5.10 | 0.08 | 15.41 | 0.07 | −71.74 | 0.01 | 2.62 | 0.02 | a |
| | | 4.30 | 0.02 | 14.46 | 0.10 | −71.74 | 0.01 | 2.94 | 0.01 | d |
| | C$^{18}$O(1-0) | 0.56 | 0.02 | 1.44 | 0.02 | −71.65 | 0.01 | 2.44 | 0.03 | b |
| | C$^{18}$O(2-1) | 1.07 | 0.03 | 3.10 | 0.02 | −72.05 | 0.01 | 2.45 | 0.02 | b |
| | | 0.96 | 0.01 | 2.89 | 0.02 | −71.75 | 0.01 | 2.54 | 0.01 | d |
| | $^{13}$C$^{18}$O(2-1) | 0.009 | 0.005 | 0.033 | 0.005 | −71.89 | 0.47 | 3.49 | 1.16 | |
| | $H_2CS(3_{1,2}$-$2_{1,1})$ | 0.090 | 0.004 | 0.22 | 0.01 | −71.75 | 0.02 | 2.30 | 0.04 | d |
| | $H_2CS(6_{1,5}$-$5_{1,4})$ | 0.127 | 0.007 | 0.33 | 0.01 | −72.10 | 0.03 | 2.52 | 0.06 | |
| 501 | $^{12}$CO(1-0) | 23.1 | 0.3 | 74.8 | 0.5 | −58.40 | 0.02 | 3.01 | 0.01 | |
| | $^{12}$CO(2-1) | 19.2 | 0.2 | 69.1 | 0.5 | −58.36 | 0.03 | 3.68 | 0.05 | a |
| | | | | | | −57.95 | 0.05 | | | c |
| | $^{13}$CO(1-0) | 5.26 | 0.02 | 11.58 | 0.02 | −58.30 | 0.01 | 1.96 | 0.01 | b |
| | | 5.58 | 0.11 | 11.95 | 0.08 | −58.49 | 0.01 | 1.95 | 0.02 | a |
| | $^{13}$CO(2-1) | 6.83 | 0.18 | 15.85 | 0.15 | −58.35 | 0.01 | 2.34 | 0.02 | a |
| | C$^{18}$O(1-0) | 0.38 | 0.02 | 0.75 | 0.01 | −58.87 | 0.02 | 1.81 | 0.04 | b |
| | C$^{18}$O(2-1) | 0.86 | 0.03 | 1.68 | 0.02 | −58.44 | 0.01 | 1.81 | 0.03 | b |

Remarks.
a - Measurements made simultaneously during maps.
b - Measurements made simultaneously during single pointed observation.
c - Peak $V_{lsr}$.
d - Measurements made simultaneously during single pointed observation ($^{13}$C$^{18}$O).
sa - Intensities and $V_{lsr}$ affected by self-absorption.

data presented by Langer & Penzias (1990; their Table 2) to compare optical depths derived from LTE calculations with those derived from their LVG models (their Table 4), and found that there are no significant differences between both methods. Both optical depths however depend on the assumed excitation (or kinetic) temperature.

Our C$^{18}$O, $^{13}$C$^{18}$O, and $H_2CS$ data towards WB 89-437 are shown in Figs. 3 and 7. The $H_2CS$ ($3_{1,2}$−$2_{1,1}$) and ($6_{1,5}$−$5_{1,4}$) lines in Figs. 7g and h were observed simultaneously with the same receivers as the $^{13}$C$^{18}$O(1−0) and (2−1) transitions, and their detections show that the tuning was correct. Because the $^{13}$C$^{18}$O(1−0) emission is expected to be very weak, we do not show a spectrum at the resolution of 0.11 km s$^{-1}$, but show in Fig. 7c a large velocity range at a resolution of 0.89 km s$^{-1}$, and in Fig. 7d this spectrum in the same velocity range as the $H_2CS$ result in Fig. 7g and for comparison the C$^{18}$O(1−0) (smoothed to the same resolution of 0.89 km s$^{-1}$) in Fig. 7a. No

**Table 4.** $^{13}CO/C^{18}O$ line ratios

| WB 89 | (1-0) ratio | | (2-1) ratio | | $T_{ex}$ | $T_{kin}$ (K) | | $\log(n_{H_2})$ | | $N(^{13}CO)$ | $N(C^{18}O)$ | Ratio |
|---|---|---|---|---|---|---|---|---|---|---|---|---|
| | $T_A^*$ | $\int T_A^* dv$ | $T_A^*$ | $\int T_A^* dv$ | K | $^{13}CO$ | $C^{18}O$ | $^{13}CO$ | $C^{18}O$ | $cm^{-2}$ | $cm^{-2}$ | |
| 380 | 9.0 | 12.2 | 8.2 | 9.8 | 22.5 | | | | | 2.10(16) | 1.58(15) | 13.3 |
| | | | | | | 22.5 | 22.5 | 3.82 | 3.74 | 8.52(15) | 5.56(14) | 15.3 |
| | | | | | | 17.5 | 12.5 | 3.93 | 4.37 | 8.52(15) | 6.66(14) | 12.8 |
| 391 | 10.2 | 12.4 | 7.7 | 9.3 | 15.5 | | | | | 9.72(15) | 6.42(14) | 15.1 |
| | | | | | | 15.5 | 15.5 | 4.01 | 4.29 | 4.01(15) | 3.67(14) | 10.9 |
| | | | | | | 12.5 | 9.5 | 4.25 | >5.00 | 4.39(15) | 3.67(14) | 12.0 |
| 399 | 13.5 | 12.6 | 12.0 | 10.2 | 20.9 | | | | | 7.70(15) | 5.55(14) | 13.9 |
| | | | | | | 20.9 | 20.9 | 4.09 | 4.09 | 3.59(15) | 2.70(14) | 13.3 |
| | | | | | | 15.9 | 10.9 | 4.61 | >5.00 | 3.93(15) | 2.70(14) | 14.6 |
| 437 | 8.6 | 10.6 | 5.4 | 6.3 | 22.3 | | | | | 2.25(16) | 1.87(15) | 12.0 |
| | | | 4.5 | 5.0 | | | | | | | | |
| | | | | | | 22.3 | 22.3 | 3.26 | 3.82 | 8.63(15) | 8.71(14) | 9.9 |
| | | | | | | 17.3 | 12.3 | 3.58 | 4.57 | 8.63(15) | 9.54(14) | 9.0 |
| 501 | 13.8 | 15.4 | 7.5 | 9.1 | 24.4 | | | | | 1.82(16) | 1.04(15) | 17.5 |
| | | | | | | 24.4 | 24.4 | 3.34 | 3.89 | 8.92(15) | 4.49(14) | 19.9 |
| | | | | | | 19.4 | 14.4 | 3.38 | 4.61 | 9.76(15) | 4.92(14) | 19.8 |

emission is visible at the expected velocity in the $^{13}C^{18}O(1-0)$ spectrum, which has an rms of 1.4 mK. A 3 mK line is visible near $-54$ km s$^{-1}$ at the expected frequency of $C_4H$ ($N$=11−10, $J$=21/2−19/2) at 104.705102 GHz. Gaussian fits to the smoothed $C^{18}O(1-0)$ spectrum give a peak temperature of 0.534±0.008 K and a line width of 2.57±0.04 km s$^{-1}$. This means a 3$\sigma$ lower limit of the $C^{18}O/^{13}C^{18}O$ ratio of 127±10. Corrections for the $C^{18}O(1-0)$ optical depth (0.03 according to our LTE analysis), and the difference in frequency between both transitions (see Eq. 1) change this lower limit to 118±10. Because the expected $^{13}C^{18}O$ line width is 2.9 channels, however, we have a formal 3$\sigma$ lower limit of the $C^{18}O/^{13}C^{18}O$ ratio of 216±16 (and a corrected value of 201±15).

The $^{13}C^{18}O(2-1)$ spectrum in Fig. 7e seems to contain a relatively strong line. However close inspection of this spectrum also shows the presence of some residual baseline ripple. After removal of this ripple by deleting one channel in the Fourier-transformed spectrum, we obtain Fig. 7f. In this spectrum (which has an rms noise of 4.8 mK) there is some suggestion of the presence of a 9 mK line. For comparison we have plotted in Fig. 7b the $C^{18}O(2-1)$ spectrum smoothed to the same resolution of 0.44 km s$^{-1}$. The ratio $C^{18}O/^{13}C^{18}O$ would be 107±60 (peak $T_A^*$) or 88±14 ($\int T_A^* dv$), which after correction would decrease slightly to 104±60 or 85±14. These values are significantly lower than the ones derived from the (1−0) transitions, a result which was also found towards W 33 and W 3OH (see below).

In Fig. 4 we show the $H_2CS$ distribution towards W 33. The line shapes and intensity distribution are almost equal to that of $C^{18}O$, suggesting that the emission of both molecules originates in the same part of the cloud. Because the individual $^{13}C^{18}O(1-0)$ spectra (except towards (0″, 24″)) are too noisy, we do not show its distribution. The observations by Langer & Penzias (1990) towards W 33 have been made with angular resolutions of 1.′7 ($C^{18}O$ and $^{13}C^{18}O$), and we convolved our map around the position (0″, 0″) to this resolution and the resulting spectra are shown in Figs. 8a to d. In the $^{13}C^{18}O(1-0)$ spectrum there is also emission from $C_4H$ ($N$=11−10, $J$=21/2−19/2) at 104.705102 GHz (at a velocity of about 53 km s$^{-1}$ in Figs. 7c and g), and from $CH_3OCH_3$ ($7_{2,6}-7_{1,7}$ AA and EE) at 104.705953 and 104.703328 GHz (at velocities of about 50.5 and 58.1 km s$^{-1}$, respectively). Probably because we did not observe the emission to the edge of the clump (and the $C^{18}O(2-1)$ spectra are undersampled), our temperatures are somewhat higher than those of Langer & Penzias. Line parameters towards W 33 are listed in Table 5. Where possible, we give integrated temperatures for the intervals used by Langer & Penzias, in addition to that for the interval 28 to 42 km s$^{-1}$, which better defines the velocities where the denser gas is found. From our data we derive a ratio $C^{18}O/^{13}C^{18}O$ of 37.4±8.0 (peak $T_A^*$) and 42.6±3.2 ($\int T_A^* dv$ from 28 to 42 km s$^{-1}$). These are equal to or only slightly higher than the observed ratios from the Langer & Penzias data of 37.6 and 39.9 (for the $V_{lsr}$ interval 26−40 km s$^{-1}$). However in view of the calibration uncertainties of both the present and Langer & Penzias' observations the difference is not significant. In Figs. 8e to j are displayed the results towards (0″, 24″), where we made a longer integration. Here we find ratios for $C^{18}O/^{13}C^{18}O$ of 37.4±3.7 (peak $T_A^*$) and 39.5±1.4 ($\int T_A^* dv$ from 28 to 42 km s$^{-1}$), which are somewhat lower than those derived from the mapped spectra, but almost equal to the values of Langer & Penzias. The correction factor (not applied by Langer & Penzias) towards (0″, 24″) using Eq. (1), would be 1.15. These authors find different ratios towards (0″, 0″) and (8′, 0′), and it is possible that the abundance ratios are not constant within the cloud.

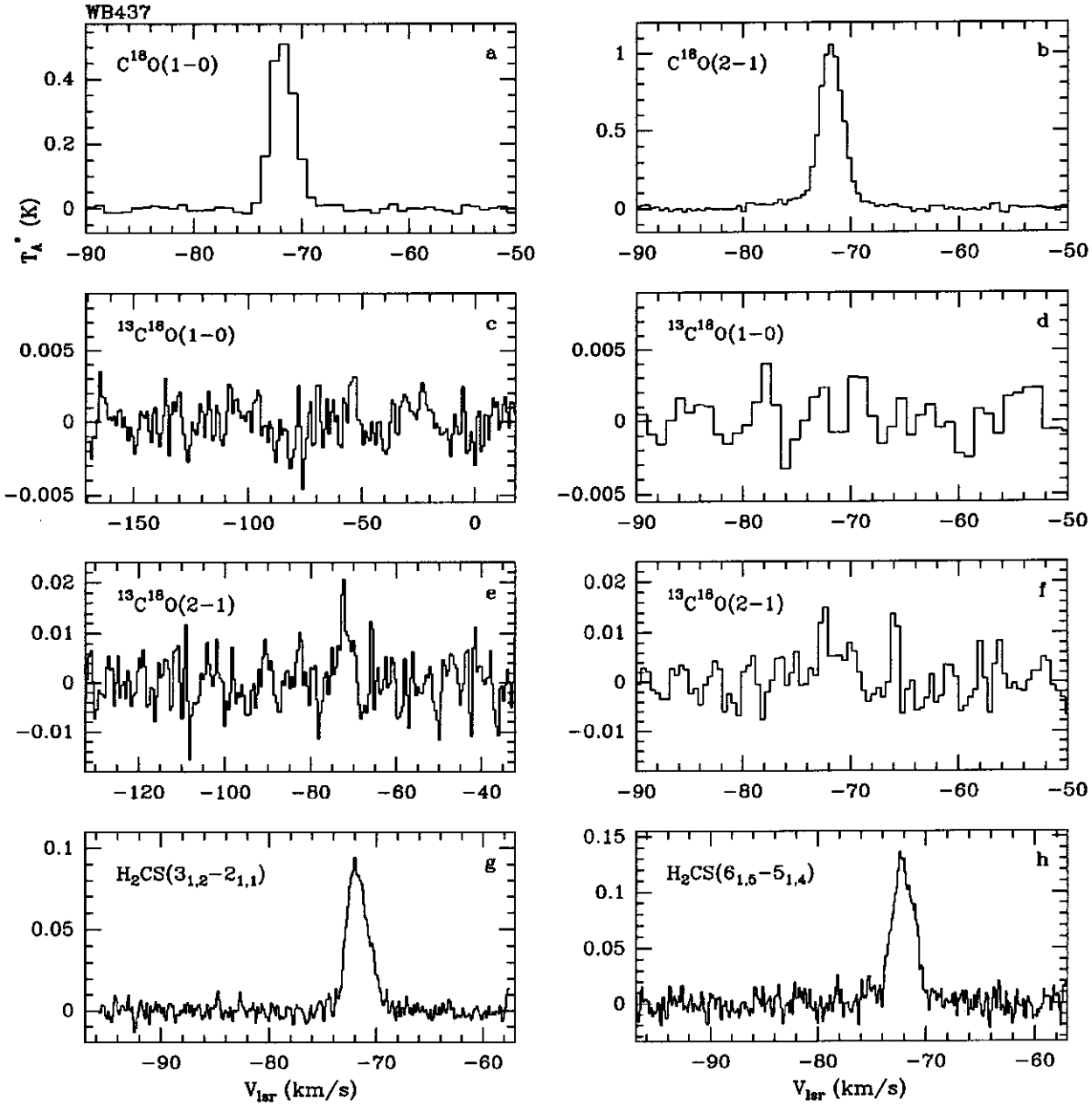


**Fig. 7.** Spectra towards WB 89-437. **a, c, d)** $C^{18}O(1-0)$ and $^{13}C^{18}O(1-0)$ at a resolution of 0.89 km s$^{-1}$. The feature in **c, d)** at about −54 km s$^{-1}$ is probably due to $C_4H$ ($N$=11−10, $J$=21/2−19/2) at 104.705102 GHz. **b, e, f)** $C^{18}O(2-1)$ and $^{13}C^{18}O(2-1)$ at a resolution of 0.44 km s$^{-1}$. $^{13}C^{18}O(2-1)$ is shown before **e**) and after **f**) removal of some baseline ripple. **g, h)** $H_2CS$ ($3_{1,2}-2_{1,1}$) and ($6_{1,5}-5_{1,4}$) at the original velocity resolution of 0.11 km s$^{-1}$

Towards (0″, 24″) we also observed $^{13}C^{18}O(2-1)$, though with relatively low signal to noise ratio (see Fig. 8i). The observed (2−1) $C^{18}O/^{13}C^{18}O$ ratios are much lower than the (1−0) values: 24.0±2.1 (peak $T_A^*$) and 25.0±1.0 ($\int T_A^* dv$ from 26 to 40 km s$^{-1}$). These differences are probably due to the much higher $C^{18}O(2-1)$ optical depths: from Eq. (1) we derive a correction factor of 1.28, which would increase the ratio to about 31±2. However it still is smaller than the ratio obtained from the (1−0) transition.

We can also use our data towards the calibration source W 3OH to derive the abundance ratio. The W 3OH spectra are shown in Fig. 9 and line parameters are listed in Table 6. The observed (1−0) line ratio is 88±15 (peak $T_A^*$) or 68±12 ($\int T_A^* dv$), which would change only little with the correction factor of 0.97. Although our $^{13}C^{18}O$

**Table 5.** W 33 line parameters

| transition | $T_A^*$ K | | $\int T_A^* dV$ Kkm s$^{-1}$ | | $V_{lsr}$ km s$^{-1}$ | | $\delta v$ km s$^{-1}$ | | Remarks |
|---|---|---|---|---|---|---|---|---|---|
| ($0''$,$0''$), convolved to $1.7'$ resolution | | | | | | | | | |
| $^{13}$CO(1-0) | 15.54 | 0.04 | 107.0 | 0.2 | 35.42 | 0.05 | 6.39 | 0.05 | b |
| | | | 123.1 | | | | | | c |
| $^{12}$CO(2-1) | 18.14 | 0.05 | 259.2 | 0.5 | 35.84 | 0.05 | 12.4 | 0.1 | d |
| | | | | | 32.9 | 0.1 | | | e |
| C$^{18}$O(1-0) | 3.85 | 0.10 | 22.68 | 0.16 | 35.34 | 0.02 | 5.68 | 0.04 | a |
| | | | 23.34 | | 35.46 | | | | b |
| C$^{18}$O(2-1) | 5.17 | 0.05 | 30.52 | 0.08 | 35.29 | 0.01 | 5.68 | 0.02 | a |
| | | | 31.21 | | 35.40 | | | | b |
| $^{13}$C$^{18}$O(1-0) | 0.103 | 0.022 | 0.532 | 0.04 | 35.28 | 0.18 | 5.26 | 0.41 | a |
| | | | 0.536 | | 35.11 | | | | b |
| $H_2CS(3_{1,2}$-$2_{1,1})$ | 0.540 | 0.021 | 2.69 | 0.03 | 35.34 | 0.03 | 4.99 | 0.07 | a |
| | | | 2.74 | | 35.50 | | | | b |
| ($0''$,$24''$) | | | | | | | | | |
| $^{13}$CO(1-0) | 22.29 | 0.08 | 151.5 | 0.5 | 35.54 | 0.05 | 6.09 | 0.05 | b |
| | | | 165.2 | 0.5 | 36.06 | 0.05 | | | c |
| | | | | | 35.66 | 0.05 | | | e |
| $^{13}$CO(2-1) | 15.93 | 0.06 | 119.02 | 0.5 | 35.32 | 0.05 | 7.04 | 0.05 | b |
| | | | 129.92 | 0.5 | 35.99 | 0.05 | | | c |
| | | | | | 35.90 | 0.05 | | | e |
| $^{12}$CO(2-1) | 21.43 | 0.07 | 284.2 | 1.0 | 35.52 | 0.05 | - | - | d,f |
| | | | | | 30.69 | 0.05 | | | e |
| C$^{18}$O(1-0) | 8.37 | 0.09 | 45.20 | 0.15 | 35.18 | 0.01 | 4.97 | 0.02 | a |
| | | | 46.17 | | 35.28 | | | | b |
| C$^{18}$O(2-1) | 10.79 | 0.08 | 63.59 | 0.12 | 34.99 | 0.01 | 5.62 | 0.01 | a |
| | | | 65.08 | | 35.14 | | | | b |
| $^{13}$C$^{18}$O(1-0) | 0.224 | 0.022 | 1.17 | 0.04 | 34.88 | 0.07 | 4.99 | 0.18 | a |
| | | | 1.17 | | 34.98 | | | | b |
| $^{13}$C$^{18}$O(2-1) | 0.45 | 0.04 | 2.54 | 0.10 | 35.11 | 0.16 | 5.31 | 0.45 | a |
| $H_2CS(3_{1,2}$-$2_{1,1})$ | 1.33 | 0.019 | 6.57 | 0.03 | 35.13 | 0.01 | 4.32 | 0.03 | a |
| | | | 6.79 | | 35.35 | | | | b |
| $H_2CS(6_{1,5}$-$5_{1,4})$ | 1.15 | 0.10 | 4.70 | 0.10 | 34.27 | 0.09 | 4.02 | 0.20 | a |

Remarks.
a - 26 to 40 km s$^{-1}$.
b - 28 to 42 km s$^{-1}$.
c - 12 to 56 km s$^{-1}$.
d - 0 to 70 km s$^{-1}$.
e - peak $V_{lsr}$.
f - complex spectrum, no linewidth given.

**Table 6.** W 3OH line parameters

| transition | $T_A^*$ K | | $\int T_A^* dV$ Kkm s$^{-1}$ | | $V_{lsr}$ km s$^{-1}$ | | $\delta v$ km s$^{-1}$ | | Remarks |
|---|---|---|---|---|---|---|---|---|---|
| $^{12}$CO(1-0) | 26.0 | 0.2 | 253.4 | 0.5 | −47.8 | 0.2 | 9.3 | 0.2 | a |
| $^{12}$CO(2-1) | 22.1 | 0.1 | 256.0 | 0.2 | −47.6 | 0.2 | 11.1 | 0.2 | a |
| $^{13}$CO(1-0) | 14.0 | 0.05 | 76.0 | 0.1 | −47.2 | 0.1 | 5.2 | 0.1 | b |
| $^{13}$CO(2-1) | 12.3 | 0.1 | 77.9 | 0.2 | −47.5 | 0.1 | 6.4 | 0.1 | b |
| C$^{18}$O(1-0) | 2.54 | 0.03 | 11.6 | 0.05 | −47.6 | 0.1 | 4.3 | 0.1 | b |
| C$^{18}$O(2-1) | 4.58 | 0.03 | 23.3 | 0.05 | −47.5 | 0.1 | 4.5 | 0.1 | b |
| $^{13}$C$^{18}$O(1-0) | 0.029 | 0.005 | 0.17 | 0.03 | −47.4 | 0.4 | 5.3 | 0.8 | |
| $^{13}$C$^{18}$O(2-1) | 0.20 | 0.04 | 1.05 | 0.25 | −48.0 | 0.4 | 5.1 | 0.7 | c |
| $H_2CS(3_{1,2}$-$2_{1,1})$ | 1.04 | 0.02 | 3.75 | 0.03 | −46.1 | 0.1 | 3.0 | 0.1 | b |
| $H_2CS(6_{1,5}$-$5_{1,4})$ | 2.52 | 0.05 | 10.4 | 0.05 | −47.5 | 0.1 | 3.4 | 0.1 | b |

Remarks.
a - −75 to −25 km s$^{-1}$.
b - −60 to −35 km s$^{-1}$.
c - confusion with $^{33}SO_2(16_{3,13}-16_{2,14})$?

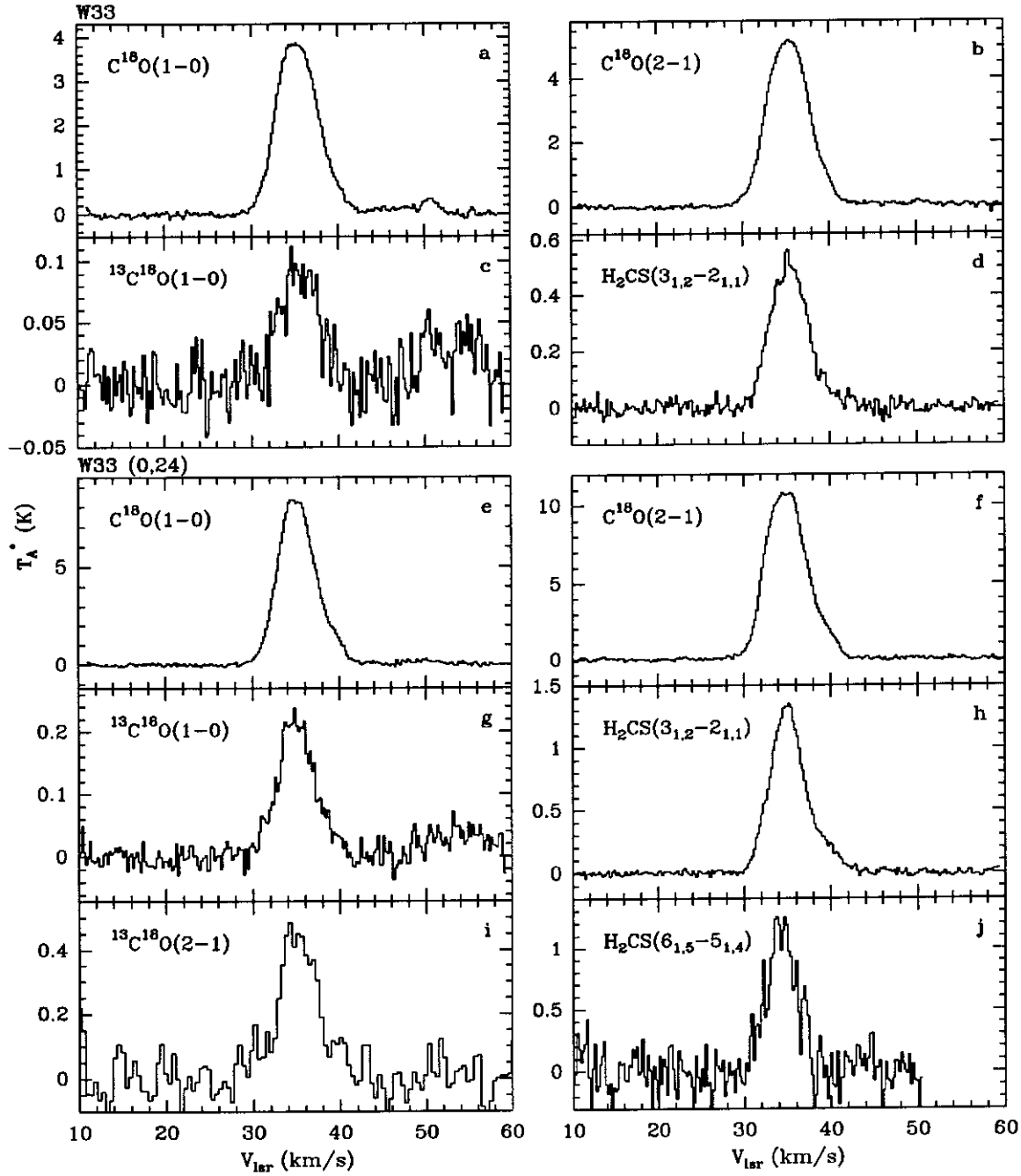


**Fig. 8.** $C^{18}O(1-0)$, $C^{18}O(2-1)$, $^{13}C^{18}O(1-0)$, and $H_2CS(3_{1,2}-2_{1,1})$ spectra in W33 towards (0″, 0″) **a to d**), convolved to the Langer & Penzias (1990) resolution of 1′.7, and towards (0″, 24″) **e to j**), unsmoothed. The velocity resolution in these spectra is 0.2 km s$^{-1}$, except $^{13}C^{18}O(2-1)$ (0.44 km s$^{-1}$)

spectrum has a low signal to noise ratio, it is in agreement with the ratios observed by Langer & Penzias (1990), 67.8 (peak $T_A^*$) and 72.7 ($\int T_A^* dv$). Also towards W 3OH the (2−1) ratios are lower than the (1−0) ratios: we find ratios of 22.9±4.6 (peak $T_A^*$) and 22.3±5.3 ($\int T_A^* dv$). The correction factor would be 1.04. Our $^{13}C^{18}O(2-1)$ spectrum in Fig. 9h also shows a line at about −55 km s$^{-1}$, which might be due to $^{33}SO_2$ ($16_{3,13}-16_{2,14}$) at 209.4255 GHz. This line (at 137.2 K above ground) is not visible towards the other sources, probably because $T_{kin}$ in W 3OH is much larger.

Our result for the ratio $C^{18}O/^{13}C^{18}O(1-0)$ towards WB 89-437 implies that the ratio $^{12}C/^{13}C$ is even larger than the number based on the extrapolated abundance

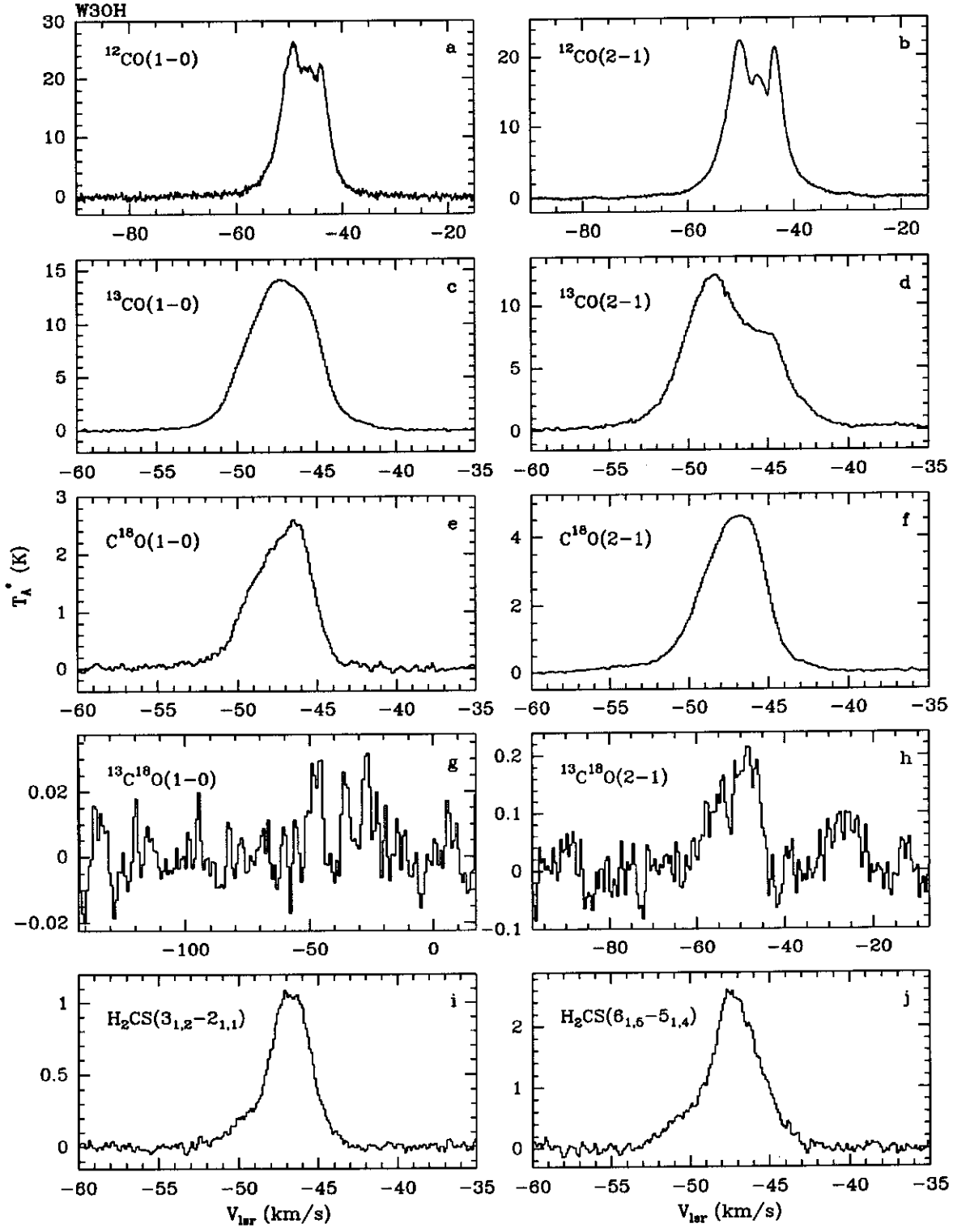


**Fig. 9.** $^{12}$CO, $^{13}$CO, C$^{18}$O, $^{13}$C$^{18}$O (1−0) and (2−1), and $H_2CS$ ($3_{1,2}-2_{1,1}$) and ($6_{1,5}-5_{1,4}$) spectra towards the calibration position in W 3OH

gradient from WM 92 (110-123). During the $^{13}C^{18}O$ observations we simultaneously observed also $C^{18}O(2-1)$ (see Sect. 4.1), and because this line was as strong as during the previously made $C^{18}O(1-0)$ observations, the absence of $^{13}C^{18}O$ emission is not caused by pointing errors. We are confident that our results towards WB 89-437 are reliable, also because our results towards W 33 and W 3OH agree with those found by Langer & Penzias (1990).

We refer to Langer & Penzias (1990, 1993) for a discussion of the uncertainties involved in the method of deriving the $^{12}C/^{13}C$ ratio from $^{12}C^{18}O$ and $^{13}C^{18}O$ data. The processes possibly affecting the abundance ratio are $^{13}C$ isotopic fractionation and self-shielding. Both processes depend on the UV radiation intensity, but work in opposite directions. Because the interstellar radiation field is expected to be much weaker at large R, and radio continuum measurements did not reveal an HII region (which would indicate the presence of embedded O stars) towards WB 89-437 (Rudolph et al. 1996), such processes will be negligible. Moreover the $^{13}C^{18}O$ emission originates in the densest part of the clouds, where the extinction is high (several tens of magnitudes) and models of high density ($10^3 < n(H_2) < 5\ 10^4$) regions (Langer & Graedel 1989) suggest that $^{13}C^{18}O$ fractionation is absent there. This is the range of densities derived for the FOG sources (see Table 4).

Langer & Penzias (1993) show that their (1−0) results for local clouds are consistent with those obtained from e.g. $CH^+$ measurements. Our deviating (2−1) results might be related to the higher critical densities for those transitions, and the radiation therefore will not originate in the same part of the cloud as the (1−0) emission. The lower level of the $H_2CS$ ($6_{1,5}-5_{1,4}$) transition is at 38.3 K above ground, and its detection suggests that the gas in the cloud core might be hotter than the temperature indicated by the $^{12}CO$ emission. $NH_3$ observations towards W3 OH, where the difference between (1−0) and (2−1) ratios is largest, indicate a $T_{\rm kin}$ of 100 K (Mauersberger et al. 1986). Without a detailed study of temperature and density distribution in the sources the contradictions cannot be resolved.

According to Matteucci & D'Antona (1991), their chemical evolution models fit best if the initial amount of $^{13}C$ is negligible and the ratio $^{12}C/^{13}C$ can be very high (>1000) in chemically young regions. Because WB 89-437 is located near the edge of the stellar disk (see e.g. Brand & Wouterloot 1995), the ratio could therefore be much higher than our lower limit. Our findings (although based on observations of only one source) are consistent with the models by WM 92, which predict that also the $^{12}C/H$ and $^{13}C/H$ ratios in the FOG are lower than in the solar neighbourhood, and therefore the interpretation by Brand & Wouterloot (1995) of apparently contradicting column densities being due to galactic abundance gradients rather than to a much lower value of $X$ (see Sect. 1), may be correct.

## 5. Conclusions

We have selected a sample of five far-outer Galaxy molecular clouds which are located at distances from the galactic centre between 16 and 17 kpc. Towards the five molecular clouds, all with an embedded IRAS source, small maps around the IRAS source were made in various isotopes and transitions of CO. From the $^{13}CO(2-1)$ maps we found representative clump sizes to be between 1 and 2 pc, and virial masses between 480 and 3600 $M_\odot$.

We observed $C^{18}O(1-0)$ and (2−1) towards the position in each source with the highest column density, which was taken to be that of the $^{13}CO$ peak. From our data we derived the ratios of $^{13}CO$ and $C^{18}O$ column densities towards the FOG sources. They are found to be about 14, which might be slightly larger than found towards local GMCs, but the interpretation of this result is unclear due to beam filling factor effects.

From our sample of sources we selected WB 89-437 as having the largest probability of showing detectable $^{13}C^{18}O$ emission, based on the intensity of the $^{12}C^{18}O$ line. Towards this source, we have obtained a $3\sigma$ lower limit of $201 \pm 15$ for the ratio $^{12}C/^{13}C$, from observations of $^{12}C^{18}O(1-0)$ and $^{13}C^{18}O(1-0)$.

At an $R$ of 16.2 kpc, WB 89-437 represents the most distant point in the Galaxy where the $^{12}C/^{13}C$ ratio has been determined; up to now the ratio had been known out to $R \approx 10.5$ kpc only (WM 92). An extrapolation of the gradient found for $R < 10.5$ kpc (WM 92) yields a ratio of 110-120 at $R \approx 17$ kpc. The present measurement seems to indicate that the gradient continues into the FOG, and may even be steeper there. It is obvious that any more quantitative statement requires more data at large R, but this is complicated by the fact that the $^{13}C^{18}O$ line is expected to be so faint that the integration times become almost prohibitively large (to reach the present rms level of 1.4 mK at a resolution of 0.89 km s$^{-1}$ required 20 hrs of on-source integration time).

WB 89-437 also exhibits a strong outflow, with a total velocity range in $^{12}CO(2-1)$ of 80 km s$^{-1}$. The stronger (blue) outflow is unresolved (<0.5 pc) in the present observations. At extreme velocities the $^{12}CO$ outflow emission becomes less optically thick and the $^{12}CO/^{13}CO$ ratio is above 100, which is larger than found towards local outflows and consistent with a larger than local $^{12}C/^{13}C$ abundance ratio in this cloud.

As comparison sources we observed the same transitions towards the core of the inner Galaxy source W 33, as well as towards W 3OH. The size at half maximum of the W 33 core is about 1.5 pc in $C^{18}O$ and the corresponding virial mass 8200 $M_\odot$. From our $J$=1−0 observations we determined peak $^{12}C/^{13}C$ ratios of 43.0±4.3 (towards

W 33) and 85±15 (towards W 3OH), which are equal to that in earlier published determinations.

Ratios $^{12}C/^{13}C$ derived from the corresponding $J$=2−1 transitions (104±60, 31±2, and 24±2 for WB 89-437, W 33, and W 3OH respectively) are significantly smaller than those derived from the $J$=1−0 transitions, a result which is not yet explained, but may be due to the emission of the two transitions originating in different parts of the cloud with different excitation conditions.

*Acknowledgements.* This work has been supported in part by the Deutsche Forschungsgemeinschaft (DFG) through grant SFB-301. We thank R. Simon (Univ. Köln) and R. Moreno (IRAM, Granada) for assistance with the September 1994 and August 1995 observations, respectively.

## References

Brand J., Wouterloot J.G.A., 1994, A&AS 103, 503
Brand J., Wouterloot J.G.A., 1995, A&A 303, 851
Castets A., Duvert G., Dutrey A., et al., 1990, A&A 234, 469
De Geus E., Brand J., Rudolph A.L., Wouterloot J.G.A., 1996, ApJ, (submitted)
Dickman R.L., 1978, ApJS 37, 407
Downes D., 1989, Radio astronomy techniques. In: Appenzeller I., Habing H.J., Léna P. (ed.) Evolution of galaxies - astronomical observations. Lect. Notes Phys. 333. p. 351
Fich M., Silkey M., 1991, ApJ 366, 107
Gardner F.F., Whiteoak J.B., 1979, MNRAS 188, 331
Goldsmith P.F., Mao, X.-J., 1983, ApJ 265, 791
Goss W.M., Matthews H.E., Winnberg A., 1978, A&A 65, 307
Henkel C., Güsten R., Gardner F.F., 1985, A&A 143, 148
Henkel C., Walmsley C.M., Wilson T.L., 1980, A&A 82, 41
Henkel C., Wilson T.L., Bieging J.H., 1982, A&A 109, 344
Henry R.B.C., Howard J.W., 1995, ApJ 438, 170
Ho P.T.P., Klein R.I., Haschick A.D., 1986, ApJ 305, 714
Langer W.D., Graedel T.E., 1989, ApJS 69, 241
Langer W.D., Penzias A.A., 1990, ApJ 357, 477
Langer W.D., Penzias A.A., 1993, ApJ 408, 539
Linke R.A., Goldsmith P.F., Wannier P.G., Wilson R.W., Penzias A.A., 1977, ApJ 214, 50
Matteucci F., D'Antona F., 1991, A&A 247, L37
Mauersberger R., Guélin M., Martín-Pintado J., et al., 1989, A&AS 79, 217
Mauersberger R., Henkel C., Wilson T.L., Walmsley C.M., 1986, A&A 162, 199
Panagia N., 1973, AJ 78, 929
Rolleston W.R.J., Dufton P.L., Fitzsimmons A., 1994, A&A 284, 72
Rudolph A.L., Simpson J.P., Haas M.R., Fich M., 1994, BAAS 26, 1477
Rudolph A.L., Brand J., de Geus E.J., Wouterloot J.G.A., 1996, ApJ 458, 653
Shaver P., McGee R.X., Newton L.M., Danks A.C., Pottasch S.R., 1983, MNRAS 204, 53
Snell R.L., Scoville N.Z., Sanders D.B., Erickson N.R., 1984, ApJ 284, 176
Stutzki J., Winnewisser G., 1985, A&A 144, 13
Taylor D.K., Dickman R.L., 1989, ApJ 341, 293
Wannier P.G., Penzias A.A., Linke R.A., Wilson R.W., 1976, ApJ 204, 26
Wilson R.W., Langer W.D., Goldsmith P.F., 1981, ApJ 243, L47
Wilson T.L., Matteucci F., 1992, A&AR 4, 1 (WM 92)
Wilson T.L., Rood R.T., 1994, ARA&A 32, 191
Wolfendale A.W., 1991, The mass of molecular gas in the Galaxy. In: James R.A. & Millar T.J. (eds.) Molecular Clouds. Cambridge Univ. Press, p. 41
Wouterloot J.G.A., Walmsley C.M., 1986, A&A 168, 237
Wouterloot J.G.A., Brand J., 1989, A&AS 80, 149 (WB 89)